入
85-6-230
高工研図書室

EUROPEAN ORGANIZATION OFR NUCLEAR RESEARCH

CERN-EP/85-77
May 17th, 1985

STUDY OF PARAMAGNETIC FLUCTUATIONS IN RARE EARTH ALUMINIUM INTERMETALLICS

O. Hartmann[a,b], E. Karlsson[a,b], R. Wäppling[a], J. Chappert[c], A. Yaouanc[c,d], L. Asch[e] and G.M. Kalvius[e].

[a]University of Uppsala, Institute of Physics, S-751 21 Uppsala, Sweden

[b]European Organization for Nuclear Research, CERN, CH-1211, Geneva, Switzerland

[c]Centre d'Etudes Nucléaires, DRF, Service de physique, 85 X, F-38041 Grenoble Cédex, France

[d]Los Alamos National Laboratory, Los Alamos, NM, USA

[e]Physik Department der Technischen Universität München, D-8046 Garching, Federal Republic of Germany

ABSTRACT

We have studied the magnetic fluctuations in the paramagnetic phase of rare-earth aluminium intermetallics of the type $(RE)Al_2$, by the method of transverse field muon spin rotation (μ^+SR). In cases with strong 4f-exchange these fluctuations slowed down notably on approaching the Curie point T_c. We attribute this slowing down to the formation of paramagnetic spin correlations which are observed to persist far above T_c. The crystallographic site for the μ^+ is discussed as well as the hyperfine field induced at this site due to interstitial electron polarization.

To be submitted for publication in the Journal of Physics F

1. INTRODUCTION

Recently a number of papers on itinerant magnets have reported the existence of paramagnetic short-range correlations (SRC) at temperatures substantially higher than the critical temperature T_c (Lynn, 1975, Hayano et al., 1978, Déportes et al., 1981, Ziebeck et al., 1981a, Brown et al., 1982). For instance in MnSi (Ziebeck et al., 1982a) SRC's exist to at least 20 T_c. These SRC's appear in all purely itinerant magnetic systems studied up to now and a theory has been developed to explain the experimental findings (Korenmann et al., 1977, Capellmann, 1979, Korenmann et al., 1979, Moriya, 1979).

In systems with localized magnetism the existence of SRC seems to depend on the studied system. For instance in Pd_2MnSn no SRC are found (Ziebeck et al., 1981b) whereas they have been reported for MnF_2, $PrAl_2$ (Silbernagel et al., 1968) and $CeAl_2$ (MacLaughlin et al., 1981). For Fe and Ni the interpretation is still under discussion (Uemura et al., 1983, Lynn, 1984). The very recent neutron scattering data on iron (Wicksted et al., 1984, Steinsvol et al., 1984) may, however, have eliminated the evidence for long range (15 Å) ferromagnetic correlations above T_c in these materials.

The methods used so far to study short range correlations in the paramagnetic phase are either neutron diffraction studies or observations based on spin relaxation. In the latter case it is important to note that correlations are best studied by a nuclear (or other) spin probe that does not belong to the paramagnetic ion itself. In intermetallic compounds such as the Rare Earth Aluminides ($REAl_2$) where one of the species (Al) is non-magnetic, the spin relaxation of the Al-nuclei depends, sensitively, on the instantaneous direction of the neighbouring paramagnetic spins, whereas a RE-nuclear spin (as seen e.g. in Perturbed Angular Correlations, PAC) mainly relaxes through hyperfine interaction with its own local RE-ion and correlations can then be observed only indirectly. Information on local correlations can, in principle, also be obtained from relaxation of spins of nuclei or particles placed in interstitial positions between magnetic atoms, such as the μ^+-spin. A μSR study of this type in the rare earth metals was first carried out by Grebinnik et al. (1979). However, no detailed conclusions concerning SRC were drawn.

In order to understand the origin of SRC in systems exibiting localized magnetism, we have studied a series of magnetic $REAl_2$'s (RE: Ce, Pr, Nd, Gd, Dy, Ho, Er and Tm) by the μSR-technique. This technique (see e.g.

Karlsson, 1982) is well suited for a systematic study of the spin relaxation down to T_c with all the rare earths. As far as other methods are concerned, several of the RE isotopes (e.g. ^{157}Gd) show strong neutron absorption and are, therefore, not accessible to neutron diffraction unless enriched material is used. The Al^{27} nuclear magnetic resonance (NMR) signal can only be detected for a few of these compounds at high temperature; $T >> T_c$ (Silbernagel et al., 1968). It will be also shown in this paper that the μ^+SR-spectra are sensitive to another range of magnetic correlation times than NMR.

The rare earth aluminides were chosen as first objects for a μ^+SR-study also because they constitute a long series of magnetically similar compounds with other properties well known from previous works (Barbara et al., 1982). In particular the electronic level structure of the rare earth ions in the crystal field is well established.

In addition to the information drawn from spin relaxation, values for the transferred hyperfine field at the muon site can also be derived, using the paramagnetic Knight shifts observed in μ^+SR.

The outline of the present paper is as follows. In section 2, we give the experimental arrangements. In section 3, the method used to analyse the data is explained and the main characteristics of these data are given. Section 4 is devoted to a discussion of magnetic and electric interactions in the μ^+-RE system as well as the possible sites occupied by the muons. Section 5 deals with the static hyperfine fields at the muon sites and in section 6 we give some elements of a qualitative theory of the positive muon depolarization function in magnetic metallic compounds and analyse our damping rate data within this theory. This allows us to obtain information on the spin-spin correlations and the μ^+ site. Section 7 contains some concluding remarks. Finally, some detailed calculations are given in an appendix Some of the material given here has already been presented at conferences (Chappert et al., 1981, Asch et al., 1983, Hartmann et al., 1984).

2. EXPERIMENTAL ARRANGEMENTS

The μ^+SR facilities at CERN require fairly large samples because of the relatively low μ^+ stopping rate. Alloys of about 50 g weight were prepared at CNRS, Grenoble, by induction levitation melting of stoichiometric amounts of 5N Al and 3N RE. Basically, our process produces polycrystalline ingots with a spherical base of diameter $\simeq$ 25 mm and a slightly cone-shaped top (Lemaire, 1967). Due to the strongly exothermic reactions, mechanical strains can break the sample in pieces and repeated meltings were sometimes necessary to obtain a good sample. No further treatments were made. The experiment on $CeAl_2$ was made on the single crystal used by Rossignol (1980). This crystal was not oriented. Some of the samples, as for instance $GdAl_2$, showed a considerable magnetic hysteresis, so that special care must be taken in interpretation of the data near T_c.

The μ^+SR measurements were made using a standard transverse field set-up with magnetic fields on the samples typically ranging from 10 mT to 500 mT. The samples were placed either in a He-flow cryostat (200 K-2 K) or a closed cycle refrigerator (400 K-10 K). The cryostat walls were kept as thin as possible to reduced the background signal. Temperatures were measured by Pt, Si or Ge thermometers and the temperature stability during each run was typically 1 K.

Transverse field μ^+SR data are usually fitted using the expression

$$N(t) = N_0 \exp(-t/\tau_\mu)\{1 + a_0 P(t)\cos(\omega_\mu t + \phi)\} + Bg \qquad (1)$$

where N(t) is the positron count-rate as a function of the time t elapsed between the entrance of the μ^+ in the sample and the detection of the positron emitted in its decay. N_0 is a normalization constant τ_μ is the μ^+ lifetime ($2.2\ 10^{-6}$ s), ϕ is the phase of the μ^+ spin rotation, which depends on the geometry of the experimental set-up, and Bg is the accidental (time-independent) background. In addition there is always another background for muons stopping in cryostat walls etc. These muons give a small signal precessing with (almost) the same frequency as those in the sample. In some of the experiments the stainless steel dummy technique described by Kehr et al. (1982) was used to determine the background signal from muons stopped outside the sample, which may represent 10-30 % of the observable

asymmetry a_0. For the $REAl_2$ compounds, the difference in frequency between muons in the sample and in the cryostat walls was often large enough to make a direct determination of the two signals in the spectrum.

The physical parameters of interest in eq. (1) are the initial asymmetry of the positron angular distribution a_0, the damping P(t) of the μ^+ spin polarization, and the Larmor precession frequency ω_μ of the μ^+ spin in the resulting field B_μ at the muon site. The frequency f is $\omega_\mu/2\pi = \gamma_\mu B_\mu$ where $\gamma_\mu = 1.3554 \times 10^8 s^{-1} T^{-1}$. The damping term P(t) is for simplicity taken to be either of Lorentzian, $P(t) = \exp(-\lambda t)$, or of Gaussian, $P(t) = \exp(-\sigma^2 t^2)$, shape, which represent the two extremes of complete motional narroving and static inhomogeneous broadening, respectively.

3. EXPERIMENTAL μ^+ SR DATA

3.1 General features

The μSR parameters were first obtained by fitting Eq. (1) to the experimental spectra, in general using a two-frequency fit without restrictions. In the cases where the two frequencies were too close together for an unambiguous fit with free parameters, the background signal had to be assumed to have temperature-independent amplitude, damping or frequency. For $DyAl_2$, $PrAl_2$ and $GdAl_2$ in fields of 100 mT or higher, unrestricted fits of all parameters was normally possible, while in $HoAl_2$, $ErAl_2$ and in most spectra at lower fields, the above limitations had sometimes to be applied. In these latter cases, where the two frequencies were not fully resolved, the data evaluation was complicated and not always unambiguous.

The following main features emerge from the transverse field spectra of the $REAl_2$ compounds:

a/ The total amplitude a_0 of the precession signal is very much reduced below T_c and the remaining asymmetry is consistent with the fraotion of muons sitting in the cryostat walls.

b/ Above T_c, the signal is characterized by a temperature and field dependent damping P(t) which is strong close to T_c, but decreases towards higher temperatures.

c/ Above T_c, a frequency shift of the sample signal can be observed in most of the samples. Close to T_c the shift is so large that the beating of the sample frequency and the cryostat frequency can be directly observed in the spectrum.

Examples of these three effects are given in figs. 1-3.

Figs 1a and 1b show the case of the polycrystalline $DyAl_2$ sample in an external magnetic field of 0.13 T. One of the two components of the signal called "background" has a fairly low asymmetry a_0 and its parameters change little in the temperature range above T_c. It also agrees well with the weak precession signal remaining at temperatures below the magnetic transition. We attribute this component to muons stopped in the cryostat walls, sample holder, etc. Below T_c the spontaneous magnetization of the ferromagnetic compounds causes a distortion of the applied magnetic field in its environment (cryostat, sample holder, etc.) and this is the reason why the "background" signal is shifted in frequency and strongly broadened below T_c. These "background" signals will not be discussed further, but they can not be neglected since they constitute an important correction for obtaining the true properties of the signal from the sample.

The sample signal in Fig. 1 shows a strongly increased damping rate when T approaches T_c from above, and this signal is lost in the ferromagnetic region. For this particular sample, there is also a strong increase in the frequency when T_c is approached. Note that in fig. 1b we present the Gaussian damping rate, which in general gives a better fit than the Lorentzi close to T_c. It should be noted that the observed damping rates are field-dependent. Fig. 2 shows a few examples of this behaviour, which also shows that the extrapolated damping rate at zero field is non-zero.

The frequency shift of the signal can have either sign. In the example shown in fig. 3 ($PrAl_2$) it is positive but in $GdAl_2$ it is strongly negative. Positive means that $B_{\mu^+} > B_{ext}$ where B_{ext} is the value of the applied external field. From the systematic study of the magnetic field and temperature dependence of the absolute value of the frequency shift, $|\Delta f|$, it is seen that $|\Delta f|$ varies linearly with $T_c/(T-T_c)$ and B_{ext}. We define a parameter k_f characterizing the frequency shift through

$$\Delta f = k_f \cdot \gamma_\mu B_{ext}/(T-T_c) \qquad (2)$$

and such a parameter k_f can be fitted for all the samples investigated. In contrast, the damping rate data can not be described by such a simple relation, and before proceeding with further fitting of the data, the origins of the frequency shifts and damping rates have to be discussed.

3.2 The magnetic field data.

As mentioned above, the muon experiences a frequency shift given by the parameter k_f. This is related to the local magnetic field sensed by the muon which can be decomposed as follows:

$$\vec{B}_\mu = \vec{B}_{ext} + \vec{B}_{cont} + \vec{B}_{dip} \tag{3}$$

where $\vec{B}_{ext}$ is the externally applied magnetic field, $\vec{B}_{cont}$ the contact field at the μ^+ and $\vec{B}_{dip}$ the total magnetic dipolar field. Magnetic correlations between the localized magnetic moments give a negligible contribution to $\vec{B}_\mu$. For $\vec{B}_{dip}$ we write:

$$\vec{B}_{dip} = \vec{B}_L + \vec{B}_{dem} + \vec{B}'_{dip} \tag{3a}$$

$\vec{B}_L$ is the Lorentz field and $\vec{B}_{dem}$ the demagnetization field. As usual, $\vec{B}_L = (4\pi/3)\vec{M}_S$ and $\vec{B}_{dem} = -\underline{N}\vec{M}$, where $\vec{M}_S$ is the saturation magnetization and $\vec{M}$ the bulk magnetization. $\underline{N}$ is the demagnetization tensor which depends only on the geometry of the sample. In the paramagnetic state one replaces $\vec{M}_S$ and $\vec{M}$ with $\vec{M}_P$ where $\vec{M}_P = \chi\vec{B}_{ext}$ and χ is the susceptibility. If the samples were of ellipsoidal shape, the sum of the first two terms of eq. (3) could be written

$$\vec{B}_L + \vec{B}_{dem} = (4\pi\frac{1}{3} - N)\chi\vec{B}_{ext} = k_M\chi\vec{B}_{ext} = k_M \frac{N_{RE}\mu_o^2\mu_B^2 g_J^2 (J+1)J}{3k(T-T_C)} \vec{B}_{ext} \tag{4}$$

$$\simeq k_M M_{eff} \frac{N_{RE}\mu_o\mu_B g_J (J+1)}{3k(T-T_C)} \vec{B}_{ext}$$

where N is given for different axial ratios (see, for instance, Zijlstra, 1967). Unfortunately, the actual shapes of our samples do not allow a simple analysis of the demagnetizing factors, but rough estimates will be given. In eq. (4) the usual high-T approximation for the susceptibility of free ions is introduced and $|M_{eff}|$ put equal to $\mu_o\mu_B g_J J$ per ion. N_{RE} is the number of RE ions per unit volume.

$\vec{B}'_{dip}$ of eq. (3a) is the dipolar magnetic field due to the 4f-magnetic moments inside the Lorentz sphere. These moments can be considered localized from the point of view of the μ^+ because the radius of the 4f-shell is $\cong$ 0.35 Å (De Gennes, 1962) whereas the distance between the shell and the μ^+ is $\cong$ 2 Å (see section 4.1) In the paramagnetic state the RE-dipoles still have a preferred orientation (although for the B_{ext} we use, their magnetization is always less than 10^{-3} of M_s), but due to the symmetry of the RE-sublattice, these fields add up to zero for each μ^+-position, and the total dipolar field will be given by eq. (4).

The contact field $\vec{B}_{cont}$ in eq. (2) is due to the spin polarization of itinerant electrons at the muon site. This polarization is caused by the f-s exchange interaction, and should be proportional to the expectation value $\langle S_z \rangle_{B_{ext},T}$ at a chosen external field and temperature, i.e. proportional to the magnetization. If crystal field effects are neglected and $\exp(-\mu_B g_J B_{ext}/k(T - T_c))$ is close to unity (which is the case for all fields applied here) the following approximate relation should hold between the muon hyperfine field $\langle B_{cont} \rangle_{B_{ext},T}$ and the saturation hyperfine field $B_{cont}(T = 0)$ expected for fully polarized R.E. moments at zero temperature in the ordered state (Goldring and Sharenberg 1958, Barash et al., 1982)

$$\vec{B}_{cont} = \frac{\mu_B g_J (J + 1) B_{cont}(T = 0)}{3k\ (T - T_c)} \cdot \vec{B}_{ext} \qquad (5)$$

This relation has been shown to be well satisfied for Al-hyperfine fields (Barash et al., 1982) in $REAl_2$, where measurements have been possible in the ferromagnetic as well as in the paramagnetic state.

The relative frequency shift is given by

$$\frac{\Delta f}{f} \equiv \frac{B_\mu - B_{ext}}{B_{ext}} = \frac{B_L + B_{dem} + B_{cont}}{B_{ext}} =$$

$$= \frac{\mu_B g_J (J + 1)}{3k(T - T_c)} [k_M M_{eff} + B_{cont}(T = 0)]. \qquad (6)$$

Since according to eq. (2), $\Delta f/f = k_f/(T-T_c)$, the contact field can be expressed as

$$B_{cont}(T = 0) = k_f \cdot \frac{3k}{\mu_B g_J (J + 1)} - k_M M_{eff} \qquad (6b)$$

However, the large uncertainty in the k_M-factors for our samples limit severely this source of information on the local spin densities at the muon sites (section 5).

3.3 The damping rate data

The magnetic fluctuations, which are the main object of the present investigation, should give a Lorentzian depolarization function in the motional narrowing limit. In the previous section, we have noted that the experimental damping rates increase strongly close to T_c, but that the rates are field dependent and that the depolarization function is closer to Gaussian in this region. This suggests that in our samples depolarization occurs by two mechanisms: (1) the field distribution caused by inhomogeneous demagnetization fields, (2) relaxation of the muons spins due to the fluctuating environment.

If these two depolarization mechanisms are independent, P(t) is given by

$$P(t) = Q_1(t) \times Q_2(t) \tag{7}$$

where $Q_1(t)$ is due to field inhomogeneity (inhomogeneous broadening) and $Q_2(t)$ describes the effect of the magnetic fluctuations.

The inhomogeneous broadening term is expected to be of the type $Q_1(t) = e^{-\sigma^2 t^2}$ with σ proportional to the susceptibility, i.e.

$$\sigma = k_1 \frac{B_{ext}}{T-T_c} \tag{8}$$

whereas $Q_2(t) = e^{-\lambda t}$ has been assumed to be independent of B_{ext}.
It was found that the damping rate data for each sample could except for $GdAl_2$ and $TmAl_2$ be well fitted with Eq. (8) plus a $Q_2(t)$- term with

$$\lambda = k_2 \cdot \frac{1}{(T-T_c)^x} = \lambda(300) \cdot \left(\frac{300-T_c}{T-T_c}\right)^x \tag{9}$$

where the exponent x varied between 0 and 0.7 (see Table I). The physical significance of this exponent is rather limited, and these fits serve mainly to obtain accurate values for the inhomogeneous broadening constant k_1.

Examples of fits with Eqs 8-9 are given in Figs 4-5, while the k_1 and x and $\lambda(300)$ parameters are found in Table I.

Extraction of the relaxation parameter λ for a more detailed temperature dependence study, $\lambda = f(T)$, can be made by extrapolating to zero in plots of damping rate versus applied field (as in fig. 2). In practice this was done by using the k_1 parameters and subtracting this broadening from the observed damping rates, which due to the different line shapes was made by numerical methods. It turns out that only the data obtained at low fields (15 mT or below) are really efficient for determining the relaxation rate, while the data from higher fields (100-130 mT) help to define the inhomogeneous broadening and the frequency shifts.

All the compounds investigated order ferromagnetically except $CeAl_2$ and $LaAl_2$. $CeAl_2$ has a modulated antiferromagnetic structure below $T_N = 3.9$ K (Barbara et al., 1979). In fig. 6, we present the data for this compound. The frequency of the "background" signal does not, contrary to the case for all the other compounds (see fig. 1a), change upon cooling below T_N. This is so because $CeAl_2$ has no spontaneous bulk magnetization and therefore no distortion of the magnetic field around the sample. This sample shows in the paramagnetic range a damping rate which decreases with increasing T. It should however be noted that NMR-work on ^{27}Al in $CeAl_2$ (McLaughlin et al., 1981) indicates a maximum at 10 K.

As a comparison we have also performed a μ^+SR experiment on $LaAl_2$, which in all respects (crystal structure,etc.) is similar to the previously mentioned compounds, except that it lacks the magnetic 4f-electrons. The results are shown in fig. 6. The damping rate should in this case only originate from the Al-nuclear dipoles. Calculations of the latter damping rate made for muons located in a typical interstitial site (see Section 5) predict $\sigma = 0.16 - 0.28\ \mu s^{-1}$. Fig. 6 includes "low field" and "high field" limits expected from the theory of Hartmann (1977). The experimental data show a considerable spread, but appear to be intermediate between the 'static muon' and the fast diffusion case. This result is unexpected since the damping rates in $PrAl_2$ and $NdAl_2$ are very close to zero above 100 K,

and it is likely that the muons are diffusing but that effects of trapping and detrapping are visible in $LaAl_2$. Even if the muon diffusion rate might be fast with respect to the muon lifetime, it is presumably not fast compared to the paramagnetic fluctuations (see section 6).

In addition to giving information about the mobility which is most probably a property shared by all sufficiently pure $REAl_2$ compounds, the $LaAl_2$ comparison also confirmed that the dominating damping mechanism in the magnetic $REAl_2$'s is due to the localized 4f-electrons; and that the direct relaxation of the μ^+ spin by interaction with the conduction electrons can be neglected.

It should also be noted that independent information on the relaxation in a few of these compounds has been obtained by the longitudinal μ^+SR technique (Kalvius et al., 1984). Furthermore measurements in transverse field on a spherical single crystal of $DyAl_2$ confirm the importance of the inhomogeneous terms for the linewidth and frequency shift data.

4. INTERACTIONS IN THE μ^+-$REAl_2$ SYSTEM

4.1 Crystallographic sites for the μ^+

The rare earth aluminides $REAl_2$ crystallise in the $MgCu_2$-type, Laves phase structure (C15). In this structure, the RE-atoms form a diamond lattice while the Al-atoms form regular tetrahedra in the interstices between the rare earths. The point symmetry of the rare earth site belongs to the cubic (T_d) group (Kirchmayer and Poldy, 1979). The structure is illustrated in fig. 7.

Measurements on a similar compound, $REFe_2$, which was charged with hydrogen (Fisch et al., 1979) have shown that at low hydrogen concentrations, the 2 Fe - 2 RE tetrahedra (the 2-2 configurations) are first occupied, then as the concentration is increased there is a successive occupation of the 3 Fe - 1 RE (the 3-1 configuration) and the 4 Fe tetrahedra (the 4-0 configuration), but octahedral interstices are never populated. Although this may serve as a guide in our interpretation, we shall have to seek independent confirmation using our own data, since Al and Fe-atoms on the lattice may not be comparable. Furthermore, the higher zero-point motion of the muon may lead to differences compared to the case of the proton. As a basis for

the further discussion, a three-dimensional cut-out section of a muon in one of the 2-2 positions is presented in fig. 8.

Fig. 7b is a [001]-projection of the unit cell showing the 16 possible 3-1 positions and the 12 possible 2-2 positions for interstitial muons (per unit cell). The 4-0 configurations (not shown) form perfect tetrahedra whereas for the 3-1 and 2-2 configurations the muon surrounding is slightly distorted

The cubic unit cell has a side length of about 8.00 Å, decreasing slowly along the series (see Table II). The μ^+-RE distance for the 2-2 configuration is about 2.10 Å and about 2.16 Å for the 3-1 configuration.
Although the experiments are performed in the paramagnetic range it is important at this point to note that the $REAl_2$ generally show considerable magnetic anisotropies. The easy axis of magnetization is [100] for $PrAl_2$, $NdAl_2$, $DyAl_2$ and $HoAl_2$ (in which case there is a change to [110] below 20 K) while $TmAl_2$ and $ErAl_2$ have [111] as the easy axis and $GdAl_2$ is isotropic (Rossignol, 1980).

4.2 The Hamiltonian for the local μ^+-RE system

The Hamiltonian can be written

$$H = H_{magn} + H_{cryst} + H_{J,ext} + H_{\mu,J} + H_{\mu,I} + H_{\mu,Q_J} + H_{\mu,ext} \qquad (10)$$

where the first two terms represent the exchange field and crystal field interactions of the RE-ions without the muon present, and the third term is the interaction of the RE-ions with the externally applied magnetic field. The last four terms represent the additional interactions introduced when the muon is present: $H_{\mu,J}$ is the magnetic interaction between the muon and the RE moments, $H_{\mu,I}$ the magnetic dipole interaction between the muon and the nuclei (Al and RE) at surrounding positions, H_{μ,Q_J} is an electric interaction caused by the electric field gradient set up at nearby RE-positions by the muon and acting on the ionic quadrupole moment Q_J, and $H_{\mu,ext}$, finally is the direct interaction of the muon magnetic moment with the external field. These interactions are illustrated in Fig. 9. We will first discuss the order of magnitude and the relative importance of these terms for the local magnetic fields and the muon relaxation.

H_{magn}: the main contribution to this term is of the form

$$-\sum_{i,j} I_{ff}\,\underline{S}_i \cdot \underline{S}_j = -2I_{ff}\sum_{i>j}\underline{S}_i \cdot \underline{S}_j = -2I_{ff}(g_J-1)^2 \sum_{i>j}\underline{J}_i \cdot \underline{J}_j \qquad (11)$$

where I_{ff} is an exchange integral over a pair of neighbouring 4f-spins and the de Gennes factor (g_J-1) is introduced when $\underline{S}$ is replaced by $\underline{J}$. In the RE-system the value of this integral is determined by the RKKY-interaction. Further contributions to H_{magn} come from the exchange interaction between each isolated 4f-spin and the conduction electrons which is of the "Korringa" form $I_{fk}\,\underline{S}_i \cdot \underline{s}_k$.

H_{cryst}: in the presence of the crystal field there will also appear terms representing the magnetocrystalline anisotropy. The single ion interaction can be deduced from the crystal field Hamiltonian (Lea et al., 1972). The crystal field interactions are relatively large with total splitting of about 200 K for $CeAl_2$, $PrAl_2$ and $NdAl_2$ and around 100 K for $DyAl_2$, $HoAl_2$, $ErAl_2$ and $TmAl_2$ (Barbara et al., 1982). The relaxation rates of the local moments may be affected by crystalline anisotropies as indicated by Barsov et al. (1984) for the case of Er-metal.

$H_{J,ext}$: the energy of the RE-moments in the external field is given by the total Zeeman splitting $\Delta E = 2J\mu_B g_J B_{ext}$, which for the maximum field applied here, 0.3 T, is of the order of 1 K. Under these conditions the precession frequency ω_j^m is about 10^{10} rad s^{-1} which is small compared to the quantity h/τ_J, where τ_J is the relaxation time of the 4f-moments. Therefore the external field and the slow muon diffusion are not expected to have any influence on the results for the RE spin dynamics.

$\mathcal{H}_{\mu,J}$: the magnetic interaction between the muon spin I_μ and the RE-angular moments $\underline{J}_i$ is a sum of dipolar and hyperfine interaction terms

$$\mathcal{H}_{\mu,J} = \mathcal{H}_{dip} + \mathcal{H}_{hf} = \sum_i \frac{\mu_o}{4\pi} \frac{\mu_N \mu_B g_\mu g_J}{r_i^3} \left[\underline{I}_\mu \cdot \underline{J}_i - 3 \frac{(\underline{I}_\mu \cdot \underline{r}_i)(\underline{J}_i \cdot \underline{r}_i)}{r_i^2} \right]$$

$$+ \sum_i A_i \underline{I}_\mu \cdot \underline{J}_i \qquad (12)$$

where $g_\mu = h\gamma_\mu/\mu_N$ and g_J are the muon and RE-ion gyromagnetic factors, $\underline{r}_i$ is the vector between the muon and the RE-ions and A_i the hyperfine interaction acting on the muon from the i:th RE ion. In general this interaction should be described by a tensor but we assume an isotropic interaction. Since both interactions are reasonably short-ranged we will take into account only the nearest neighbour RE's at the same distance d having, therefore, the same $A_i = A$.

The dipolar strength measured by the parameter

$$a = \frac{\mu_o}{4\pi} \frac{\mu_N \mu_B g_\mu}{d^3} g_J \qquad (12a)$$

is of the order of 0.01 K or 10^{-26}J. The corresponding dipolar fields are about 1 T. The hyperfine fields at the muon sites are in the range 0.1-0.4 T as will be evaluated from eq. (6) and the hyperfine interaction described by the parameter A is therefore usually smaller than the dipolar strength a.

$\mathcal{H}_{\mu,I}$ is the dipolar interaction between the muon and nearby nuclei. It is about thousand times weaker than $\mathcal{H}_{\mu,J}$ and can be neglected in the presence of the fluctuating RE-moments. Its influence on the damping rate when there are no f-electrons was measured in the case of $LaAl_2$ (fig. 6).

$\mathcal{H}_{\mu,Q_J}$ is of the form (Abragam and Bleaney, 1970)

$$\mathcal{H}_{\mu,Q_J} = B_2^0 \left[3(J_{z'})^2 - J(J+1) \right] \qquad (13)$$

where z' refers to the axis of the electric field gradient, EFG, (along the line $\underline{r}_i$ connecting the μ^+ and the RE-ion). This adds a term of different symmetry to the local electric interaction $\mathcal{H}_{cryst}$ for ions close to the muon. The factor B_2^0 is proportional to the 4f quadrupole moment expressed

through the factors $\langle r_f^2 \rangle \langle J||\alpha||J \rangle$ (Stevens, 1953) and to the EFG produced at the RE site by the muon $q = e_{eff}/2\pi\varepsilon_0 d^3$ where e_{eff} is the μ^+ effective charge.

Values estimated for B_2^0 are very uncertain because the muon charge in a metal is strongly screened, which reduces the effective charge (as seen from a distance of about 2 Å it may be reduced to one tenth of its free value). On the other hand it is expected that Sternheimer corrections associated with "outer electrons" (5d and 6s) in the RE-ions amplify the EFG on the 4f-shell by relatively large factors. By Mössbauer spectroscopy on ^{161}Dy in Dy-metal with a near neighbour vacancy, which has an effect similar to a positively charged particle, Kikkert and Niesen (to be published) have estimated $B_2^0 = 2.4$ K. Keeping q constant over the series one obtains estimates for B_2^0 and the overall splitting $\Delta Q \simeq 3B_2^0 J^2$ as given in table III. Except for $GdAl_2$ these fields are thus expected to be relatively strong.

In analogy with the EFG effect on the nuclear quadrupole moment (Hartmann, 1977), the interaction $\mathcal{H}_{\mu,Q_J}$ will influence the dynamics of the 4f-moments if the precession frequency ω_J^e around the EFG-axis is comparable to or larger than their relaxation rates (or equivalently, if the level separation caused by $\mathcal{H}_{\mu,Q_J}$ is larger than h/τ_J), as was first discussed by Schilliaci et al. (1984). As pointed out by Campbell (1984) a negative Stevens factor, as for instance for the Dy-ion, will result in a preference for the 4f-moment to lie perpendicular to the axis linking the RE-atom and the muon (cf. fig. 8) If $\tau_J \gtrsim 10^{-12}$ s, electric field splittings of the order of a 100 K could have an appreciable effect on the relaxation rates.

$\mathcal{H}_{\mu,ext}$: in the fields applied the muon precession frequencies lie in the range $\omega_\mu = 10^7 - 10^8$ s^{-1}.

5. THE HYPERFINE FIELDS

The hyperfine field sensed by the muon is a contact field. The values derived from k_f and eq. (6b) are plotted in fig. 10 (upper part). The value of the parameters of this expression for each sample is given in table IV. The demagnetization field corrections have very large limits of error which are reflected in the vertical bars. The polycrystalline sample of $DyAl_2$ was found to be partially cracked making the magnetic field inhomogeneous and the determination of the actual magnitude of the field uncertain. The preliminary results from the spherical crystal of $DyAl_2$, which need no demagnetization correction, indicate a value close to zero for the contact field for this compound.

The lower part of fig. 10 illustrates the theoretically expected dependence on the number of 4f-electrons. The s-electrons at the muon site are exchange polarized by the f-s interaction expressed by the integral I_{fs}. The hyperfine field can be written

$$B_{cont} = C\ (g_J - 1)\ J\ I_{fs} \qquad (14)$$

where the factor $(g_J - 1)$ comes from the projection of $\underline{S}_f$ (table II) on $\underline{J}_f$. This trend is plotted in the lower part of fig. 10 for I_{fs} = constant (filled circles). We have normalized to the $GdAl_2$ data ($I_{fs}(Gd) \equiv 1$ and $B_{cont}(Gd) \equiv 1$).

However, it is known from previous work an Al-nuclei in $REAl_2$ that the exchange integral decreases in an approximately linear way along the series. Taking empirical values from Kaplan et al. (1973) leads to the trend represented by the open circles in fig. 10. The agreement is satisfactory.

The contact field can be expressed (Jena, 1979) through the up-down electron spin density difference at the muon site and the spin density enhancement factor η for the muon (or proton)

$$B_{cont} = -\frac{2\mu_o}{3}\mu_B.\eta(n\uparrow - n\downarrow) \qquad (15)$$

when $n\uparrow$ and $n\downarrow$ are the interstitial electron densities (in absence of the muon) for spin up and spin down, respectively. The quantity $(n\uparrow - n\downarrow)$ is (in LS-coupling) proportional to $(g_J-1)J\ I_{fs}$.

Interstitial spin densities have been measured for several of the $REAl_2$'s by diffuse neutron scattering. In fig. 11, we have reproduced the density map for $NdAl_2$ (Boucherle et al., 1981). In the plane represented in fig. 11 there are 2 muon positions of the 2-2 and 2 of the 3-1 type (compare figs. 7 and 8). Using our result for the frequency shift in $NdAl_2$ and the result of Boucherle et al. (1981) ($\mu_B(n\uparrow - n\downarrow) = (5 \pm 2)\ 10^{-3}\ \mu_B\text{Å}^{-3}$) we get $\eta = 2(1)$ for the 2-2 position. A similar evaluation assuming the 3-1 position leads to a negative spin-density enhancement. No theoretical predictions exist so far for η in these materials.

6. THE SPIN RELAXATION

The muon spin relaxes mainly through interactions with the RE-ions. If the coupling strengths are known, the μ^+ SR data can be used to derive properties of the RE spin dynamics.

6.1 The relaxation mechanisms

From the first terms of eqs. (12) and (12a) for the dipole interaction and the estimates of the hyperfine fields made in the previous section, we get a dipolar field produced by the RE moments of ~ 1 T (Table IV), which completely dominates the hyperfine field (except for $GdAl_2$). The fields produced by the nuclear dipoles can always be neglected when paramagnetic moments are present.

The depolarization of the μ^+ spin has, in the case of a fast fluctuation of the RE angular momenta J, an exponential time-dependence characterized by the parameter λ. In our transverse field experiments λ is equivalent to the transverse relaxation rate T_2^{-1} defined in standard NMR theory (Moriya, 1956)

$$\lambda = \frac{1}{T_2} = \left(\frac{\mu_N g_\mu}{\hbar}\right)^2 \int_0^\infty d\tau \left[\phi_{zz}(\tau) + \frac{\cos(\omega_\mu \tau)}{2}(\phi_{xx}(\tau) + \phi_{yy}(\tau))\right] \qquad (16)$$

where ω_μ is the angular frequency of the muon in the applied magnetic field and the $\phi_{\alpha\alpha}(\tau)$ for α = x, y or z are symmetrized correlation functions for the magnetic field resulting from eq. (12).

$$\phi_{\alpha\alpha}(\tau) = \frac{1}{2}\left[\langle B_\alpha(\tau)\, B_\alpha(0)\rangle + \langle B_\alpha(0)\, B_\alpha(\tau)\rangle\right] \equiv \langle\{B_\alpha(\tau), B_\alpha(0)\}\rangle \qquad (17)$$

The applied magnetic field is parallel to the z direction and its effect on the expression for λ can be neglected. Since the precession angle $\omega_\mu \tau$ in the applied field during the period of the correlation time τ_J of the RE-moments is small, the cosine term in eg. (16) is close to unity. In this limit the relaxation rate due to the hyperfine interaction can be written in the case of cubic symmetry (since $B_i = A_{i-i} J_i / \mu_N g_\mu$):

$$\lambda^{(h)} = 2\left(\frac{A}{\hbar}\right)^2 \sum_{i,j} \int_0^\infty d\tau \langle\{J_{iz}(\tau), J_{jz}(0)\}\rangle \qquad (18)$$

The dipolar interaction, which has a different symmetry, contains an $\underline{I} \cdot \underline{J}$ term producing the same type of expression as in eq. (18) (with A replaced by a) When there are no correlations between different spins (i.e. with only j = i terms), and if it is sufficient to include only the $\alpha = z$ term in the dipole interaction then the addition of the tensor part of H_{dip} has the effect that the product a^2 is replaced by 3/5 a^2 when integration over all angles is carried out for the polycrystalline case. Omission of the non-secular terms ($\alpha = x,y$) is a valid approximation for nuclear dipoles since they usually relax very slowly compared to their precession period in typical external fields (which means that a probe spin sees only the z-component of the nuclear dipole field). In the case of paramagnetic moments, however, the effects of non-secular terms have to be included which means a further multiplication with the factor 10/3, as discussed for instance by Tanaka and Tomita (1963).

The relaxation rate due to the dipole fields must therefore in our case (cubic symmetry) be written

$$\lambda^{(d)} = \frac{3}{5} \cdot 2 \cdot \frac{10}{3} \left(\frac{a}{\hbar}\right)^2 \Sigma_{i,j} \int_0^\infty d\tau \langle\{J_{iz}(\tau), J_{jz}(0)\}\rangle \qquad (19)$$

A more complete proof of the multiplication is sketched in appendix A. The hypothesis used to derive eqs. (18) and (19) are further discussed in the same appendix. The values of a and A are presented in table V for μ^+ in $REAl_2$. The a-values have been calculated with eq. (12a) using free ion moments (which are close to the experimental magnetic moments)

The same μ^+-RE distance for the two sites proposed have been used for the whole series (based on 8.000 Å for the side of the unit cube) although in reality it is slightly decreasing in size over the series. The hyperfine interaction constants are those obtained from the frequency shifts in this work. The latter are important in order to get the total rate λ only for $GdAl_2$ in which case the coupling constant X^2 replacing a^2 in eq. (19) is $(a^2 + A^2/2)$. For all others we can put $\lambda = \lambda^{(d)}$.

For the 3-1 configuration λ depends only on the auto-correlation function $\langle\{J_z(\tau), J_z(0)\}\rangle$ of <u>one</u> RE-ion

$$\lambda\ (3\text{-}1)\ = \frac{4a^2}{\pi^2} \int_0^\infty d\tau \langle\{J_z(\tau), J_z(0)\}\rangle \qquad (20)$$

while for the 2-2 configuration we have, since the two RE-ions are equivalent,

$$\lambda\ (2\text{-}2)\ = \frac{4a^2}{\pi^2} \int_0^\infty d\tau \left[\langle\{J_{1z}(\tau), J_{1z}(0)\}\rangle + \langle\{J_{2z}(\tau), J_{2z}(0)\}\rangle + \right.$$

$$\left. + \langle\{J_{1z}(\tau), J_{2z}(0)\}\rangle + \langle\{J_{2z}(\tau), J_{1z}(0)\}\rangle\right]$$

$$= \frac{8a^2}{\pi^2} \left[\int_0^\infty d\tau \langle\{J_z(\tau), J_z(0)\}\rangle + \int_0^\infty d\tau \langle\{J_{1z}(\tau), J_{2z}(0)\}\rangle\right] \qquad (21)$$

In the (2-2) case the interstitial probe measures, in addition to the self-correlation function, also the local pair correlation function for the spins 1 and 2.

The correlation functions are thermal averages over the density matrix of the magnetic ions. In our systems, the RKKY coupling to other 4f spins and the coupling of the 4f spin to the conduction electrons may produce J-relaxation rates of the same order of magnitude. These rates are simply additive. As indicated in fig. 9 there is also a direct J-J dipolar interaction but it is negligible in the present context.

If a short-time approximation is used then the time-dependence can be separated out (following Moriya, 1956)

$$\langle\{J_{iz}(\tau), J_{jz}(0)\}\rangle = \langle\{J_{iz}(0), J_{jz}(0)\}\rangle \exp\left[-\frac{\omega_{ff}^2 \tau^2}{2}\right] \qquad (22)$$

where

$$\langle\{J_{iz}(0), J_{jz}(0)\}\rangle = \frac{\mathrm{Tr}\{J_{iz} J_{jz} \exp(-H'/kT)\}}{\mathrm{Tr}\{\exp-(H'/kT)\}} \qquad (23)$$

where $H' = H_{magn} + H_{J,\,ext} + H_{cryst} + H_{\mu Q_J}$. For J-relaxation through the RKKY interaction the frequency ω_{ff} is proportional to the strength of the exchange coupling I_{ff}. In the high temperature approximation we have for the exchange interaction frequency

$$\omega_{ff} = \sqrt{\frac{8I_{ff}^2(g_J-1)^4 zJ(J+1)}{3\hbar^2}} \tag{24}$$

where z is the number of nearest RE-ions surrounding each RE (z=4 for $REAl_2$).

In a mean field approximation, when $H_{cryst} = 0$, we have (Kittel, 1971, modified for J instead of S)

$$I_{ff} = \delta \frac{3k\theta_p}{2z(g_J-1)^2 J(J+1)} \tag{25}$$

In our case $\theta_p \cong T_c$. The factor δ depends on the actual lattice and typical values are 1.5-2, In the present calculation we have chosen $\delta = 2$. Using the high temperature limit for the self-correlation we have:

$$\int_0^\infty d\tau \langle \{J_z(\tau), J_z(0)\} \rangle = \frac{1}{3} J(J+1) \sqrt{\frac{\pi}{2}} \frac{1}{\omega_{ff}} \tag{26}$$

We expect therefore, <u>if no correlations are present and only RKKY-relaxation acts</u> on the RE-moments, that

$$\lambda = n.\frac{4a^2}{\hbar^2} \frac{1}{3} J(J+1) (\tau_J)_{ff} \tag{27a}$$

$$(\tau_J)_{ff} = \sqrt{\frac{\pi}{2}} \frac{1}{\omega_{ff}} \tag{27b}$$

where n = 1 for the 3-1 and n = 2 for the 2-2 positions.

The quantities I_{ff} as deduced from the Curie temperatures of the different $REAl_2$'s (eq. (25)) are presented in table V together with the $(\tau_J)_{ff}$ and λ-values expected assuming RKKY interaction only and muons in the 2-2 tetrahedral sites. If the muons were in the 3-1 sites, the λ-values expected would be reduced by a factor of 2. These λ-limits are expected to be temperature independent down to the region where correlations between the directions of neighbouring spins become important.

The Korringa mechanism is determined by the coupling strength $I_{fk}\underline{J} \cdot \underline{s}$ where s is a conduction electron spin and the following expression for the relaxation time of the RE-ions due to interactions with conduction electrons has been used (strictly valid only for spin J = 1/2).

$$(\tau_J)_{fk} = \frac{\hbar}{\pi[I_{fk}N_F(0)]^2 kT} \qquad (28)$$

where $N_F(0)$ is the density of electrons at the Fermi surface for one direction of the conduction electron spin. The de Gennes factor is included in I_{fk}. The value derived from Loewenhaupt (1983) which gives, with the present definition of I_{fk}, $|I_{fk}N_F(0)| = 0.08(4)$ is used for the whole series of $REAl_2$'s.

In the presence of the Korringa mechanism the effective relaxation time for the 4f-moments is computed from the relation

$$\tau_J = \frac{1}{(\tau_J)_{ff}^{-1} + (\tau_J)_{fk}^{-1}} = \frac{1}{C_1 T_c \sqrt{\frac{3}{J(J+1)}} + \frac{\pi}{\hbar}[I_{fk}N_F(0)]^2 kT} \qquad (29)$$

since the two rates can be added. The quantity $(\tau_J)_{fk}^{-1}$ is proportional to the temperature T, whereas $(\tau_J)_{ff}^{-1}$ is T-independent in the absence of correlations: hence the variation of λ with temperature will have the shape indicated in figures 12-14 for different values of the parameters $|I_{fk}N_F(0)|$. The value of the constant $C_1 = 1.477 \cdot 10^{11}\ s^{-1}\ K^{-1}$

For temperatures very close to T_c the correlation functions are expected to increase as $(T-T_c)^x$ due to the presence of the many-body correlations leading to magnetic ordering at T_c. For the critical fluctuations in the temperature range $(T - T_c)/T_c < 0.01$, scaling theory predicts $x = -1.00$

A PAC-experiment using the hyperfine field of ^{100}Rh nuclei (Gottlieb and Hohenemser, 1973) implanted in Ni-metal gave x = 0.70 (3) in this temperature range.

If the muons in $REAl_2$ are sitting in the 2-2 positions, as will be argued in the next section, the second term in eq. (21) gives a possibility to observe the T-dependence of the pair correlation function $<\{J_{iz}(\tau),J_{jz}(0)\}>$. The pair correlations are expected to exist at temperatures higher than those for the long range order since they are only part of the total many-body interaction. They may therefore show a less pronounced critical behaviour than the bulk properties (compare calculations by Lindgård (1982) for other RE-systems). The pair correlation is superimposed on a "background" consisting of the T-independent term of the self-correlation function.

Eq. (21) shows an advantage of using interstitial muons as spin probes: the study of RE nuclear spin would only give the self-correlation part of the spin dynamics since the hyperfine interaction with its own 4f-shell is completely dominating.

6.2 Discussion of results from the muon relaxation

The experimental values of λ, as deduced by subtracting the inhomogenous broadening term by the procedures mentioned in section 4 are presented in figs. 12-14.

As mentioned in section 3.3 the damping rates for three of the samples, $PrAl_2$, $GdAl_2$ and $DyAl_2$ have also been measured using the zero-field μ^+SR technique (Kalvius et al., 1984). The results for the absolute values and the temperature dependence of the dampings are in good agreement with those derived here. The latter experiment measures the T_1-relaxation, but for the relaxation rates encountered, $T_1 = T_2$.

The relaxation rates for the lighter $REAl_2$'s (Pr and Nd) are small and, with the errors arising from the subtraction procedure, hardly distinguishable from the background. Low values are expected from eq. (27) remembering that λ is proportional to $g_J^2[J(J+1)]^{3/2}$. The Curie temperatures are comparable to those of $HoAl_2$ and $DyAl_2$.

The λ (T) curve for $GdAl_2$ remains relatively high even when the temperature is raised above 1.5 T_c.

The corresponding curves for $DyAl_2$ and $ErAl_2$ show large muon relaxation rates near T_c, but a general decrease with temperature. On the contrary $HoAl_2$ shows a relatively weak T-dependence. This can also be seen from the x-values in Table I.

The quantitative comparison with eqs. (27) and (29) can be seen from table V and the λ(T)-figures. The limits expected when only the RKKY-interaction is considered are indicated by horizontal lines expected for muons in the 2-2 positions when no correlations are taken into account. The Korringa relaxation introduces a T-dependence through eq. (29) for τ_J. For $GdAl_2$, this dependence is weak in the temperature range studied, since $(\tau_J)_{ff}^{-1}$ is dominating, but it is noticable in $DyAl_2$ where the Korringa relaxation changes the expected damping rates at high temperatures according to the lines drawn for three values of the quantity $|I_{fk}N_F(0)|$. For $HoAl_2$ and $ErAl_2$ Korringa relaxation becomes dominant and determines the shape of the curves.

The special case of $CeAl_2$ (antiferromagnet in the ordered state) is in reasonable agreement with expectations as far as λ is concerned. The results indicate a weaker T-dependence than should be expected for the Korringa relaxation alone. An antiferromagnetic J_1-J_2 correlation above T_N might be present.

Figs 12-14 give support for a 2-2 assignment for the μ^+ position. The fits also agree reasonabely well with the values for $|I_{fk}N_F(0)|$ derived from Loewenhaupt. But before one can extract with confidence the product $|I_{fk}N_F(0)|$ from the μ^+SR data, the model has to be refined.

6.3 RE spin correlations

In table V and figs. 12-14 it can be seen that the model described by eq. (29) does not explain all the features of the experimental data, particularly $DyAl_2$ and $GdAl_2$. This indicates the existence of spin correlations. In the other cases, correlation effects have not been observed with certainty, either because of the dominance of the Korringa relaxation or the difficulties in deducing the relaxation part of the muon depolarization near T_c.

The correlations seem to persist to high temperatures (in terms of T/T_c) both in $DyAl_2$ and in $GdAl_2$. As far as the pair correlation term is concerned a tentative explanation of this difference can be obtained by writing eq. (21) in the form (compare eq. (26)).

$$\lambda\ (2\text{-}2) = \frac{8a^2}{\hbar^2}\left[\ \frac{1}{3}\,J(J+1)\,\tau_J + \langle\{J_{1z}(0),J_{2z}(0)\}\rangle\,(\tau_J)_{\text{pair}}\right] \qquad (30)$$

Evaluation of the correlation function at high temperatures gives:

$$\langle\{J_{1z}(0),J_{2z}(0)\}\rangle = \frac{2I_{ff}}{kT}\,(g_J-1)^2\,\left[\frac{1}{3}\,J(J+1)\right]^2 \qquad (31)$$

and using eq. (25), with $z = 4$ and $\delta = 2$,

$$\langle\{J_{1z}(0),J_{2z}(0)\}\rangle = \frac{1}{3}\,J(J+1)\,\frac{\delta}{z}\,\frac{T_c}{T} \simeq \frac{1}{3}\,J(J+1)\,\frac{T_c}{2T} \qquad (32)$$

If $(\tau_J)_{pair} \simeq \tau_J$ the temperature dependence of λ should have the form

$$\lambda \simeq \lambda_{uncorr} \left(1 + \frac{T_c}{2T}\right) \qquad (33)$$

which is included for $DyAl_2$ and $GdAl_2$ in Fig. 14. A similar result has been derived by Silbernagel et al. (1968) using another approach. The remaining difference for $DyAl_2$ can be understood in terms of a stronger T-dependence for $(\tau_J)_{pair}$ than for τ_J (as calculated for EuO by Lindgård (1983)). For $GdAl_2$ the measured relaxation rates also remain large compared to the value predicted ($\lambda = 0.11\ \mu s^{-1}$) at $T = 2\ T_c$ without correlations. The high level of λ observed in our experiments is however consistent with the $DyAl_2$ data (which is seen when λ is plotted as function of T/T_c for both cases, see fig. 14).It is also evident from the interpretation given above that the correlation effects are observable only when the RKKY interaction is strong enough (high T_c) to dominate in the $(\tau_J)^{-1}$ rate over the Korringa mechanism.

An alternative way to explain these data is to take into account crystal anisotropy that may help to stabilize the pair correlation along certain axes. With an axial model for H', the evalutation of the traces would give a strong T-dependence for the self-correlation term in eq. (21). However Gd-ions in $GdAl_2$, in contrast to Dy-ions in $DyAl_2$, are known to have a very small anisotropy and they should not be influenced by any orientational dependence of the correlation function. An indication of a possible crystal field dependence is given by the recent observations (Kalvius et al., to be published) that DyAg, which shows antiferromagnetic ordering and has different crystal field parameters but a similar T_c as compared to $DyAl_2$, shows a $\lambda(T)$ starting from the same high-T level, but increasing more slowly on approaching T_c than in $DyAl_2$.

6.4 Influence of the muon on the RE spin dynamics

In the comparison of the strengths of magnetic coupling between the different spins, I_μ, I_{Al}, J_i, J_j and s we have noticed that for the RE angular momenta J, the coupling to the muon spin I_μ is negligible in comparison to the coupling to other J's and to the conduction electrons. The presence of the muon does not, therefore, perturb the $REAl_2$ system in this respect.

As pointed out in section 4.2 the electric coupling may, on the other hand, be important if the EFG set up by the muon charge at neighbouring RE ions reaches the same order of magnitude as the crystalline field (CEF) normally acting on the ions. If the EFG is stronger than the crystal field, this leads to a precession of the RE angular momentum along the axis linking the μ^+ and the RE-ion. The fundamental frequency of such a precession, ω_J^e, can be calculated from the values of B_2^0 (which themselves are very crude estimates) to be of the order of $10^{11} - 10^{12}$ s^{-1}, which means that $\underline{J}$ would make one complete period in a time interval of $\cong 10^{-10} - 10^{-11}$ s. If this time is shorter than the corresponding period in the normal crystalline field and also shorter than τ_J, the relaxation time in the absence of the muon, then the RE spin system would be perturbed by the probe particle. An alternative way of comparison is to compare the overall electric field splittings due to the muon EFG and the CEF. This is done in table III. It is noticed that the action of the muon EFG should be particularly large for Pr and Ce ions because of their large $\langle J||\alpha||J\rangle \cdot \langle r_f^2 \rangle$ factors.

As is known for the case of the nuclear dipole interaction, an axial EFG caused by muons will always reduce the effective second moment of the dipolar interaction for polycrystalline samples and thus lower the damping rate from its "free moment"-value. Since the latter seems to be well reproduced for instance in the case of Dy at high temperature, we have an indication that both of the electric precession periods are in fact long compared to τ_J in that case (and also in Gd which has no ionic quadrupole moment). On the other hand, for situations with a combination of long τ_J, small inherent splitting, observation at low temperature, and large $\langle J||\alpha||J\rangle \langle r_f^2 \rangle$ factor the effect may become important. The presence of the muon would in such cases destroy the correlations between the spins near the μ^+ and the ones far away from it. Correlations of the spins nearest to the μ^+ are still possible because they are all disturbed in the same way by the μ^+.

Fig. 15 summarizes the characteristic times involved in this study of the $REAl_2$ systems. If the RE relaxation rates are small, they might be affected by the presence of the muon, but they are in general expected to be independent of its diffusion (each muon spends a time long compared to τ_J in each position between jumps) and of the applied field.

7. CONCLUSIONS

The present set of experiments have shown that it is possible to employ the μ^+SR-method to study details of spin dynamics in metallic RE-systems, in a time-range which is hardly accessible to any other method. Effects of short range correlations have been observed in the $DyAl_2$ and $GdAl_2$ cases and their temperature range has been found to be fairly estended above T_c. For orther RE Al_2-systems studied here the relaxation of the paramagnetic moments are either dominated by the Korringa relaxation ($ErAl_2$, $HoAl_2$ and probably also $TmAl_2$) or the instantaneous fields at the muon sites are too weak for such effects to be detected ($PrAl_2$, $NdAl_2$) to be detected ($PrAl_2$, $NdAl_2$). The pair correlation term is not sufficient to explain the T-dependence. The formalism for higher order terms in the short range correlations has not yet been developed.

Possible effects of the crystalline fields and of the perturbation by the muon on the local magnetic properties have been discussed, but are found to be of minor importance, at least in the high temperature range valid for $DyAl_2$ and $GdAl_2$ (where τ_J is small, $< 10^{-12}$s).

Another set of data, obtained from the same experiments is related to the spin polarization at the interstitial positions occupied by the muons. These data may be compared to calculations of electron screening of hydrogen-like particles in these intermetallic systems, and thus support information on properties of hydrogen in the $REAl_2$ systems. A specific piece of information in this respect are the positions of the μ^+. The present study indicates that they are situated in the centres of tetrahedra composed of 2 RE- and 2 Al-atoms.

Technically, this first study suffers in several respects from low accuracy due to difficulties in sample preparation, a problem which can be overcome in future experiments, so that the possibilities of the method can be fully utilized.

ACKNOWLEDGEMENTS

Among several persons who have participated part-time we especially thank Lars Olov Norlin and Ewa Wäckelgård. The help of R. Perrier de la Bathie (CNRS Grenoble) for the preparation of the polycrystalline samples is gratefully acknowledged. This work was financially supported by NFR (Sveden), BMFT (FRG) and DOE (USA).

APPENDIX A

In this appendix, we express the transverse relaxation rate, λ in terms of spin-correlation functions. For simplicity we assume that the μ^+ is coupled only to its nearest nighbour magnetic ions.

The magnetic interaction between the μ^+ spin I_μ and the RE-angular momenta J_i is given by eq. (12) and can be written:

$$H_{\mu J} = -\mu_N g_\mu (I_{\mu z} B_z + \frac{1}{2} I_{\mu +} B_- + \frac{1}{2} I_{\mu -} B_+) \tag{A1}$$

where

$$B_z = -\frac{\mu_B g_J \mu_0}{d^3 4\pi} \sum_m \{J_{mz}(1 - 3\cos^2\theta_m + \gamma)$$

$$- \frac{3}{2} J_{m+} \sin\theta_m \cos\theta_m e^{-i\Phi_m} - \frac{3}{2} J_{m-} \sin\theta_m \cos\theta_m e^{+i\Phi_m}\} \tag{A2}$$

$$B_- = -\frac{\mu_B g_J \mu_0}{d^3 4\pi} \sum_m \{-3J_{mz} \sin\theta_m \cos\theta_m e^{-i\Phi_m} \tag{A3}$$

$$- \frac{3}{2} J_{m+} \sin^2\theta_m e^{-2i\Phi_m} + J_{m-} (\frac{3\cos^2\theta_m - 1}{2} + \gamma)\}$$

$$B_+ = B_-^* \tag{A4}$$

where ϕ_m and θ_m are the azimuthal and polar angles of ion m and $\gamma \equiv A/a$ (see section 5B). μ_o is the magnetic permeability of vacuum (SI units). We will assume that the μ^+ diffusion is slow (compare Fig. 15). Therefore, the angles are time independent. For simplicity, we will neglect also pair correlations. Then, from the definition of the magnetic field correlation function (eq. (17)), we get:

$$\phi_{zz}(\tau) = \left(\frac{\mu_B g_J \mu_0}{d^3 4\pi}\right)^2 \sum_m \{(1 - 3\cos^2\theta_m + \gamma)^2 \Lambda^{zz}_{mm}(\tau)$$

$$+ \frac{9}{2} \sin^2\theta_m \cos^2\theta_m (\Lambda^{xx}_{mm}(\tau) + \Lambda^{yy}_{mm}(\tau))\}$$

$$\phi_{xx}(\tau) + \phi_{yy}(\tau) = \left(\frac{\mu_B g_J \mu_0}{d^3 4\pi}\right)^2 \sum_m \{9\sin^2\theta_m \cos^2\theta_m \Lambda^{zz}_{mm}(\tau)$$

$$+ \left[\frac{9}{4} \sin^4\theta_m + \left(\frac{3\cos^2\theta_m - 1}{2} + \gamma\right)^2\right] \left[\Lambda^{xx}_{mm}(\tau) + \Lambda^{yy}_{mm}(\tau)\right]\}$$

where $\Lambda^{\alpha\alpha}_{mm}(\tau) = \langle\{J_{m\alpha}(\tau), J_{m\alpha}(0)\}\rangle$ is the α component of the spin-correlation function for ion m. In these expressions we neglect non-diagonal spin correlation function, as for example $\Lambda^{z+}_{mm}(\tau)$, because within the short-line approximation (eq. 22) they vanish.

$\Lambda^{\alpha\alpha}_{mm}(\tau)$ does not depend on α if for instance the ion m is in a cubic environment. Then, using eq, (19) for a polycrystal we obtain:

$$\lambda = \frac{2na^2(\gamma^2 + 2)}{\hbar^2} \int_0^\infty d\tau \, \Lambda^{zz}(\tau)$$

Therefore, the total relaxation rate is equal to the sum of the dipolar and hyperfine rate. The interference term is proportional to $(1-3\cos^2\theta)$ which is zero for a polycrystal.

If the pair-correlations are considered, one obtains eq. (21) for $\lambda^{(h)}$. The dipolar rate depends on $(\theta_m - \theta_n)$ and $(\Phi_m - \Phi_n)$. But qualitatively eq. (19) should be valid.

REFERENCES

- Abragam A and Bleaney B 1970 Electron Paramagnetic Resonances of Transition Ions (Clarendon Press).
- Asch L, Chappert J, Hartmann O, Kalvius G M, Karlsson E, Norlin L O, Wäppling R and Yaouanc A 1983 J. Magn. Magn. Mat. 31-34 697.
- Barash Y B, Barak J and Kaplan N 1982 Phys. Rev. B25 6616.
- Barbara B, Rossignol M F, Boucherle J X, Schweizer J and Buevoz J L 1979 J. Appl. Phys. 50 2300.
- Barbara B, Murani A and Rossignol M F 1982 J. Phys. F12 2625.
- Barth H J, Netz G, Nishiyama K and Riegel D 1981 Hyp. Int. 10 811.
- Boucherle J X 1977 Thèse, Université de Grenoble.
- Boucherle J X and Schweizer J 1981 J. Magn. Magn. Mat. 24 308.
- Borghini M, Niinikoski T O, Soulie J C, Hartmann O, Karlsson E, Kehr K W, Richter D and Walker E 1978 Phys. Rev. Lett. 40 1723.
- Brown P J, Capellmann H, Déportes J, Givord D and Ziebeck K R A 1982 J. Magn. Magn. Mat. 30 243.
- Campbell I A 1984 J. Phys. (Paris) 45 L27.
- Capellmann H 1979 Z. Phys. B34 29.
- Chappert J. Kalvius G.M. Asch L, Yaouanc A, Hartmann O, Norlin L O and Karlsson E 1981 Hyp. Int. 9 595.
- De Gennes P G 1962 J. Phys. et Le Rad. 23 510.
- Déportes J, Givord D and Ziebeck K R A 1981 J. Appl. Phys. 52 2074.
- Fisch G E, Rhyne J J, Sankar S G and Wallace W E 1979 J. Appl. Phys. 50 2003.
- Furrer A and Purwins H G 1977 Physica 86-88B 189.
- Goldring G and Scharenberg R P 1958 Phys. Rev. 110 701.
- Gottlieb A and Hohenemser 1973 Phys. Rev. Lett. 31 1222.
- Grebinnik V G, Gurevich I I, Zhulov V A, Nikol'skii V A, Selivanov V I and Suetin V A 1979 Sov. Phys. JETP 49 1100.
- Hartmann O 1977 Phys. Rev. Lett. 39 832.

- Hartmann O, Karlsson E, Wäppling R, Chappert J, Yaouanc A, Asch L and Kalvius G M 1984 Hyp. Int. 17/18/19 491.
- Hayano R S, Uemura Y J, Imazato J, Nishida N and Yamazaki T 1978 Phys. Rev. Lett. 41 1743.
- Jena P, Hyperfine Interactions 1979 Hyp. Int. 6 5.
- Kalvius G M, Nishiyama K, Nagamine K, Yamazaki T, Chappert J, Hartmann O, Karlsson E, Wäppling R, Yaouanc A and Asch L 1984 Hyp. Int. 17/18/19 497.
- Kaplan N, Dorman E, Buschow K H J and Lebenbaum D 1973 Phys. Rev. B7 40.
- Kehr K W, Richter D, Welter J M, Hartmann O, Karlsson E, Norlin L O, Niinikoski T O and Yaouanc A 1982 Phys. Rev. B26 567.
- Kikkert P J and Niesen L to be published.
- Kirchmayr R A and Poldy C A 1979 Handbook of the Physics and Chemistry of Rare Earth Chapter 14, edited by Gscneidner K A and Eyring L (North Holland).
- Kittel C 1971 Introduction to Solid State Physics, fourth edition (J Wiley and Son).
- Korenmann V, Murray J L and Prange R E 1977 Phys, Rev. B16 4032 4048 4058.
- Korenmann V and Prange R E 1979 Phys. Rev. B19 4091 4698.
- Lea K R, Leask M J M and Wolf W P 1962 J. Phys. Chem. Solids 23 1381.
- Lemaire R 1967 Thèse, Université de Grenoble.
- Lindgård Per-Anker 1983 Phys. Rev. B27 2980.
- Loewenhaupt M, Frick B, Walker U and Holland-Moritz E 1983 J. Magn. Magn. Mat. 31-34 187.
- Lynn J W 1975 Phys. Rev. B11 2614.
- Lynn J W 1984 Phys. Rev. Lett. 52 775.
- MacLaughlin D E, Pena O and Lysak M 1981 Phys. Rev. B23 1039.
- Maetz C J, Gerhardt U, Dietz E, Ziegler A and Jelitto R J 1982 Phys. Rev. Lett. 48 1686.

- Moriya T 1956 Prog. Theor. Phys. 16 41.

- Moriya T 1979 J. Magn. Magn. Mat. 14 1.

- Rossignol M F 1980 Thèse, Université de Grenoble.

- Schillaci M E, Heffner R. H. Hutson R L, Leon M, Cooke D W, Yaouanc A, Dodds S A, Richards P M, MacLaughlin D E and Boekema C 1984 Hyp. Int. 17/18/19 351.

- Silbernagel B G, Jaccarino V, Pincus P and Wernick J H 1968 Phys. Rev. Lett. 20 1091.

- Tomita K and Tamaka M 1963 Prog. Theor. Phys. 29 528.

- Steinsvoll Ø, Majkrzak C F, Shirane G and Wicksted J 1983 Phys. Rev. Lett. 51 300.

- Stevens K W H 1951, Proc. Phys. Soc. LXV, 209.

- Uemura Y J, Shirane G, Steinsvoll Ø and Wicksted J 1983 Phys. Rev. Lett. 51 2322.

- Wallace W E and Mader K H 1968 J. Chem. Phys. 48 84.

- Wicksted J P, Shirane G and Steinsvoll Ø 1984 Phys. Rev. B29 488.

- Yaouanc A 1984 Hyp. Int. 17/18/19 355.

- Ziebeck K R A, Brown P J, Booth P J and Bland J A C 1981a J. Phys. F11 L127.

- Ziebeck K R A, Webster P J, Brown P J and Bland J A C 1981b J. Magn. Magn. Mat. 24 258.

- Zijlstra H 1967 Experimental Methods in Magnetism, edited by Wohlfarth E P (North Holland).

Figure captions

Fig. 1 Results of the initial fits of the μSR spectra from $DyAl_2$ in 135 mT external magnetic field. The fits were made to Eq. (1) with two frequency components and all parameters free. The damping factors were taken to be Gaussians, $\exp(-\sigma^2 t^2)$, which is a good approximation below 200 K. The apparent change of amplitudes a_o at higher temperatures is not a true effect, but a consequence of the fact that the signal shape changes and that the two frequencies lie very close together.

Fig. 2. Examples of the field dependence of the observed damping rates. Far above T_c the dependence is weak as in a) $DyAl_2$ 295 K or b) $TmAl_2$ 295 K, while closer to T_c it is quite pronounced as in c) $TmAl_2$ 25 K.

The broken lines are only guides to the eye.

Fig. 3. Frequency shifts in $PrAl_2$ as function of temperature and magnetic field The shift is closely proportional to $B_{ext}/(T-T_c)$.

Fig. 4. Examples of experimental damping rates as function of temperature and magnetic field. The solid lines are fits to eqs (8-9).

Fig. 5. Temperature and field dependence of the damping rates in $TmAl_2$ and $GdAl_2$. Although the general behavour is similar to that of the other compounds, the fits to eqs (8-9) are less convincing.

Fig. 6. Measured damping rates in $CeAl_2$ and $LaAl_2$. In $LaAl_2$ the theoretical damping rates for immobile muons in interstitial sites 2-2 and 3-1 are shown. They are calculated from the nuclear dipole moments of surrounding Al and La atoms. The lower limit for each position is valid if the magnetic field dominates, the upper limit if the electric field gradient from the muon dominates.

Fig. 7. Crystallographic structure of the $REAl_2$ compounds, a) position of the rare earth and aluminium ions in a unit cell, b)[001] projection of the unit cell. Two possible types of μ^+ sites are indicated.

Fig. 8. Local surrounding of a μ^+ in one of the 2-2 positions (centre of a tetrahedron formed by two RE-ions and two Al).

Fig. 9. Schematic drawing of the different spins involved in the problem and their mutual interactions.

Fig. 10. μ^+ contact field data for the $REAl_2$ series; a) B_{cont} values extracted from the frequency shifts for μ^+ in the $REAl_2$ compounds (for $DyAl_2$, see comments in Table IV), b) variation of B_{cont} over the series expected from eq. (14). The constant C is chosen to agree with the experimental value for $GdAl_2$. The open circles are for constant I_{fk}, the filled ones if I_{fk} is allowed to decrease along the series as suggested by Kaplan et al (1973).

Fig. 11. Magnetization density in the [110]- plane of Nd Al_2 as determined by diffuse neutron scattering (Boucherle et al. 1981). The possible 1-3 and 2-2 positions of the μ^+ in this plane are indicated.

Fig. 12 a) Muon relaxation times in $HoAl_2$ after correction for the inhomogeneous broadening. More data points exist at 130 mT (below 65 K) and at higher fields, but they do not help in the determination of λ since the errors in λ get excessively large. The theoretical lines have been calculated for 3 values of the Korringa interaction given by the integral $/I_{fk}\ N(0)/$ assuming 2-2 sites for the muons.

Fig. 12 b) Same quantities as in Fig. 12 a) plotted for $PrAl_2$ and $NdAl_2$. Values on the theoretical lines indicate $/I_{fk}\ N(0)/$ with the same assumptions as above.

Fig. 13. Muon relaxation times, corrected for inhomogeneous broadening for $DyAl_2$ (upper) and $ErAl_2$ (lower). Notations and assumptions are the same as in Fig. 12.

Fig. 14. Comparison of muon relaxation rates in $DyAl_2$ and $GdAl_2$. For $DyAl_2$, results from several runs with a spherical single crystal have been added to those of Fig. 13; for $GdAl_2$ the results obtained by the zero-field method (Kalvius et al. 1984) have also been introduced. The full lines are theoretical expectations for 2-2 positions of the muons. The levels expected at $/I_{fk}\ N(0)/ = 0$ for 3-1 positions are also indicated. The dashed lines are values expected for pair correlations only (in the approximation of eq. (32), assuming $/I_{fk}\ N(0)/ = 0.08$). For comparison, the temperature scale has been chosen in units of T_c. For $GdAl_2$ the λ-values obtained at 13 mT are probably too high since the assumption of linear field dependence might not be correct (cf. Fig. 5).

Fig. 15. Characteristic times in $REAl_2$ compounds and comparison between different experimental techniques.

$(\tau_J)_{RE}$ fluctuation time of the RE ion.

$(\tau_c)_{diff}$ diffusion correlation time of the μ^+ in the $REAl_2$ compounds.

$2\pi/\omega_J^m$ Precession period in an applied magnetic field on the RE ion of $B_{ext} = \hbar\omega_B^m/\mu_B g_J$

$2\pi/\omega_J^e$ Precession period in an energy difference between crystal field levels of $\hbar\omega_c^e$.

Table captions

Table I. Results of the fits of eqs (8)-(9) to the experimental damping rates and of eq. (2) to the frequency shifts.

The parameters k_f and k_1' measure the relative field shift and the relative field distribution (rms-value), respectively. They are of the same order of magnitude.

The damping parameters are given in the unit conventionally used in μSR ($10^6 s^{-1} = \mu s^{-1}$). The T_c values are those used in the fits. Errors given are purely statistical. The quality of the damping rate fits is not very good for $GdAl_2$ and $TmAl_2$.

Table II. Lattice parameters for the $REAl_2$ compounds and properties of the RE-ions in their 3^+ state. The experimental magnetic moments are taken from Boucherle (1977).

Table III. Parameters for estimates on the electric field gradients (EFG)) on the RE-ions. The first two columns give the ground terms and the total splitting (from Barbara, Murani and Rossignol, 1982), the third the Steven's (1953) factors. The last two columns are theoretical estimates for the B_2^o-coefficient of eq. (13) and the total splitting, ΔQ, based on Dy-metal-vacancy studies (Kikkert and Niesen). No error limits can be given on these values. For $GdAl_2$ the values are taken from Schilliaci et al (1984).

Table. IV. Measured frequency shift parameters k_f and derived hyperfine (contact) fields from eq. (6b). The quantity M_{eff} is put equal to $\mu_o g_J J \mu_B$ (free ion value) except for the cases of $ErAl_2$ and $TmAl_2$ where experimental M_{eff} valurs have also been used (derived values marked by *). c/a is ellipsoidal axis ratio used for the demagnetization correction.

Table V. Quantities used for calculation of the theoretical relaxation rates. The value of a^2 in eq. (19) has been replaced by $X = (a^2 + A^2/2)$ only for the case of $GdAl_2$. The values $(\tau_J)_{ff}$ and $\lambda_{ff}(2-2)$ are those expected for the RKKY-interaction only, whereas in τ_J and $\lambda(2-2)$ the expected contribution from the Korringa relaxation has also been introduced through eq. (29) using the value $|I_{fk}N_F(0)| = 0.08$. This makes $\lambda(2-2)$ temperature dependent and the last columns present the comparison between the theoretical and measured λ-values at 300 K. Values marked by **) are based on μ_{exp} of Table II.

Table I

	T_c [K]	Damping rate data				Frequency shifts
		k_1 [$\mu s^{-1} KT^{-1}$]	$\lambda(300)$ [μs^{-1}]	x	$k_1' = k_1\sqrt{2}/2\pi\gamma_\mu$ [K]	k_f [K]
$PrAl_2$	30	68(4)	0.05(3)	0.35(12)	0.11(1)	0.12(1)
$NdAl_2$	78	67(4)	0.02(3)	0.0	0.11(1)	0.14(10)
$GdAl_2$	160	300(50)	0.38(6)	0.00(11)	0.50(8)	-0.27(5)
$DyAl_2$	67	810(80)	1.05(7)	0.70(5)	1.34(12)	1.27(10) (see text)
$HoAl_2$	32	830(40)	1.16(8)	0.00(5)	1.38(7)	0.30(4)
$ErAl_2$	14	980(80)	0.84(5)	0.72(5)	1.63(12)	0.39(9)
$TmAl_2$	6	400(60)	0.43(4)	0.02(6)	0.66(11)	-0.15(6)

Table II

	Lattice parameter (Å)	S	L	J	g_J	$g_J J$	μ_{exp} (μ_B)	Easy axis of magnetization
$LaAl_2$	8.145	-	-	-	-	-	-	non-magn.
$CeAl_2$	8.059	1/2	3	5/2	6/7	2.14	0.8	anti-ferro.
$PrAl_2$	8.025	1	5	4	4/5	3.20	2.88	[100]
$NdAl_2$	8.000	3/2	6	9/2	8/11	3.28	2.45	[100]
$GdAl_2$	7.900	7/2	0	7/2	2	7.0	7.10	
$DyAl_2$	7.840	5/2	5	15/2	4/3	10.0	9.89	[100]
$HoAl_2$	7.813	2	6	8	5/4	10.0	9.18	[100]
$ErAl_2$	7.795	3/2	6	15/2	6/5	9.0	7.80	[111]
$TmAl_2$	7.780	6	5	6	7/6	7.0	4.6	[111]

Table III

	CEF		$\langle r_f^2 \rangle \langle J \| \| \alpha \| \| J \rangle$ [a.u.]	EFG from μ^+	
	Ground term	Total splitting [K]		$\lvert B_2^0 \rvert$ [K]	ΔQ [K]
$CeAl_2$	$^2\Gamma_7$	180	$-6.8 * 10^{-2}$	34	612
$PrAl_2$	$^2\Gamma_3$	200	$-2.3 * 10^{-2}$	11.3	475
$NdAl_2$	$^2\Gamma_6$	200	$-6.4 * 10^{-3}$	3.1	186
$GdAl_2$	-	-	-	0.06	2.2
$DyAl_2$	$^4\Gamma_8^{(3)}$	100	$-4.7 * 10^{-3}$	2.4	400
$HoAl_2$	$^3\Gamma_5^{(1)}$	90	$-1.5 * 10^{-3}$	0.64	123
$ErAl_2$	$^4\Gamma_8^{(3)}$	110	$+1.7 * 10^{-3}$	0.83	142
$TmAl_2$	$^3\Gamma_5^{(1)}$	100	$+6.9 * 10^{-3}$	3.0	324

Table IV

	k_f [K]	$k_M M_{eff} + B_{cont}(T=0)$ [T]	M_{eff} [T]	$k_M M_{eff}$ [T] c/a = 1.6(±0.4)	$B_{cont}(T=0)$ [T]	notes
$PrAl_2$	0.12(1)	0.135(12)	0.0460	0.06 ± 0.03	+0.07(3)	
$NdAl_2$	0.14(1)	0.153(13)	0.0474	0.07 ± 0.03	+0.08(4)	data at 111 mT
$GdAl_2$	-0.27(5)	-0.11(2)	0.105	$0.15^{+0.05}_{-0.08}$	-0.26(9)	data at 111 mT
$DyAl_2$	1.27(10)	0.50(4)	0.154	$0.21^{+0.08}_{-0.11}$	[+0.33(12)]	standard sample
	0.00(5)	0.00(2)		0.00	0.00(2)	spherical crystal
$HoAl_2$	0.30(4)	0.120(12)	0.156	$0.21^{+0.07}_{-0.11}$	-0.09(11)	
$ErAl_2$	0.39(9)	0.170(30)	0.141 (0.122)*	$0.19^{+0.07}_{-0.10}$	-0.02(10) (0.00)*	data at 111 mT
$TmAl_2$	-0.15(6)	-0.08(3)	0.110 (0.073)*	$0.15^{+0.06}_{-0.08}$	-0.25(10) (-0.20)*	

Table V

	$\frac{1}{3}J(J+1)$	a(dip) $[10^{-27}J]$	A(hf) $[10^{-27}J]$	X^2 $[10^{-54}J^2]$	$(\tau_J)_{ff}$ $[10^{-12}s]$	$\lambda_{ff}(2\text{-}2)$ $[\mu s]^{-1}$	τ_J at 300 K $[10^{-12}s]$	λ (2-2) at 300 K $[\mu s]^{-1}$	λ_{exp} at 300 K $[\mu s]^{-1}$
$CeAl_2$	2.916	7.49	≈ 0	56.1	2.64	0.23	0.86	0.07	0.04(2)
$PrAl_2$	6.666	7.00	≈ 0	49	0.564	0.133	0:39	0.09	0.05(3)
$NdAl_2$	8.25	6.36	≈ 0	40.4	0.246	0.059	0.19	0.04	0.02(3)
$GdAl_2$	5.25	17.5	6(2)	324	0.096	0.11	0.089	0.11	0.38(6)*
$DyAl_2$	21.25	11.7	≈ 0	137	0.458	0.96	0.34	0.71	1.05(7)
$HoAl_2$	24.00	10.9	≈ 0	119	1.04	2.14	0.57	1.17	1.16(8)
$ErAl_2$	21.25	10.5	≈ 0	110 (82)**	2.23	3.76 (2.82)**	0.81	1.36 (1.02)**	0.84(5)
$TmAl_2$	14.00	10.2	≈ 0	104 (45)**	4.22	4.42 (1.91)**	0.98	1.02 (0.44)**	0.43(4)

* cf. λ_{exp} (300 K) = 0.22(6) μs^{-1} from zero field experiments (Kalvius et al., 1984)

** using empirical values of μ_J

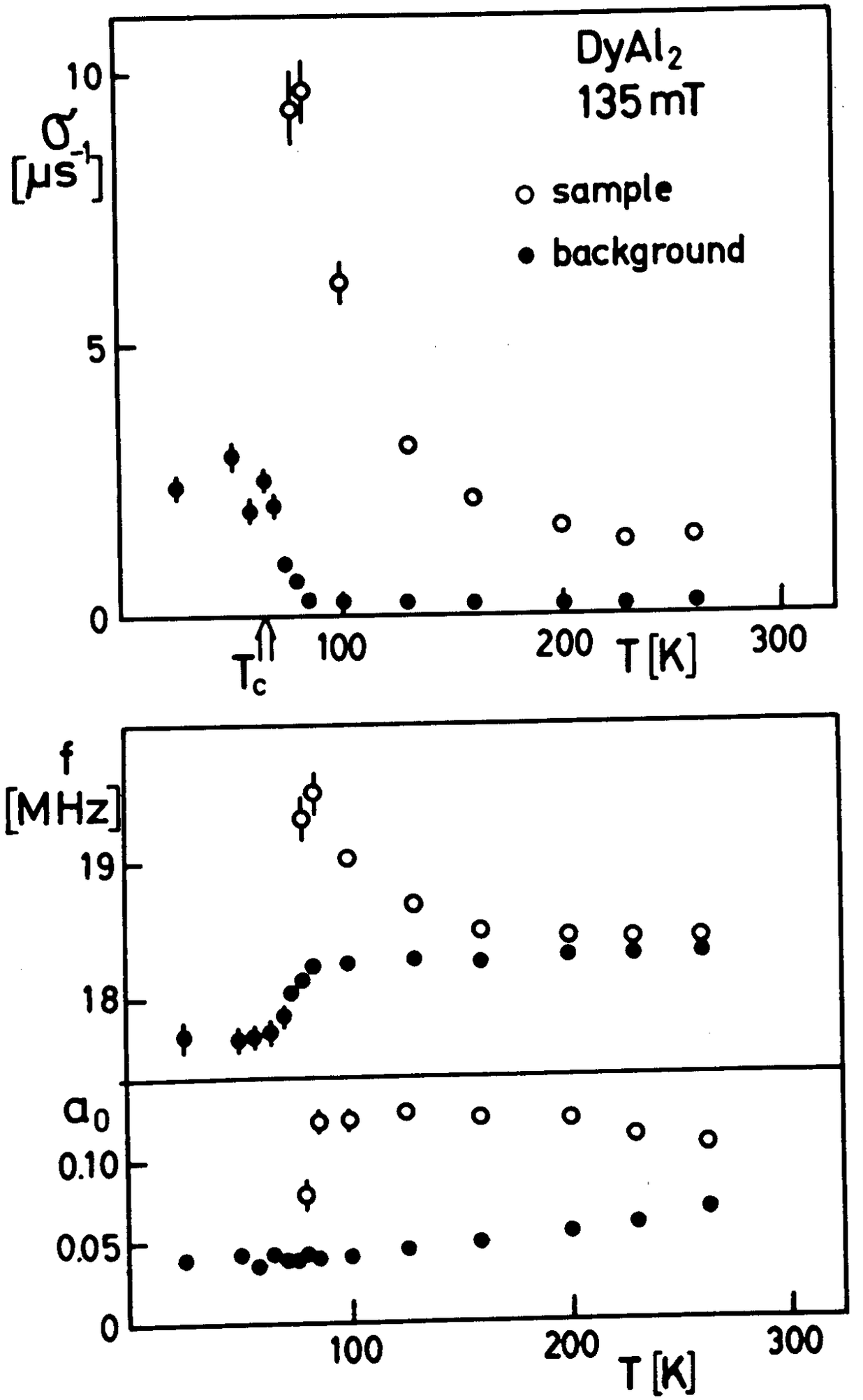
DyAl2
135 mT
sample
background
σ
[μs-1]
10
5
0
Tc
100
200
T [K]
300
f
[MHz]
19
18
a0
0.10
0.05
0
100
200
T [K]
300

FIG.1

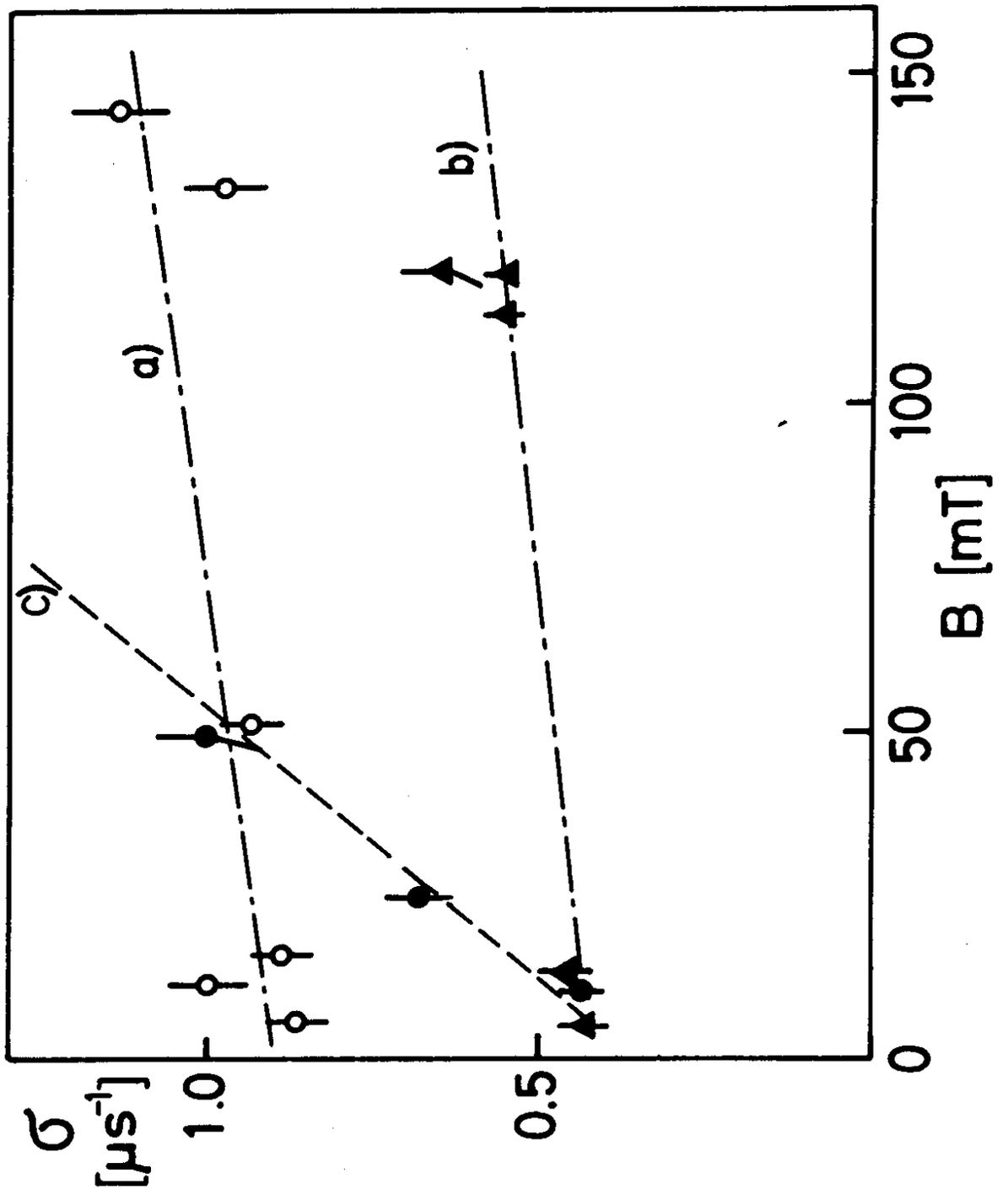

FIG.2

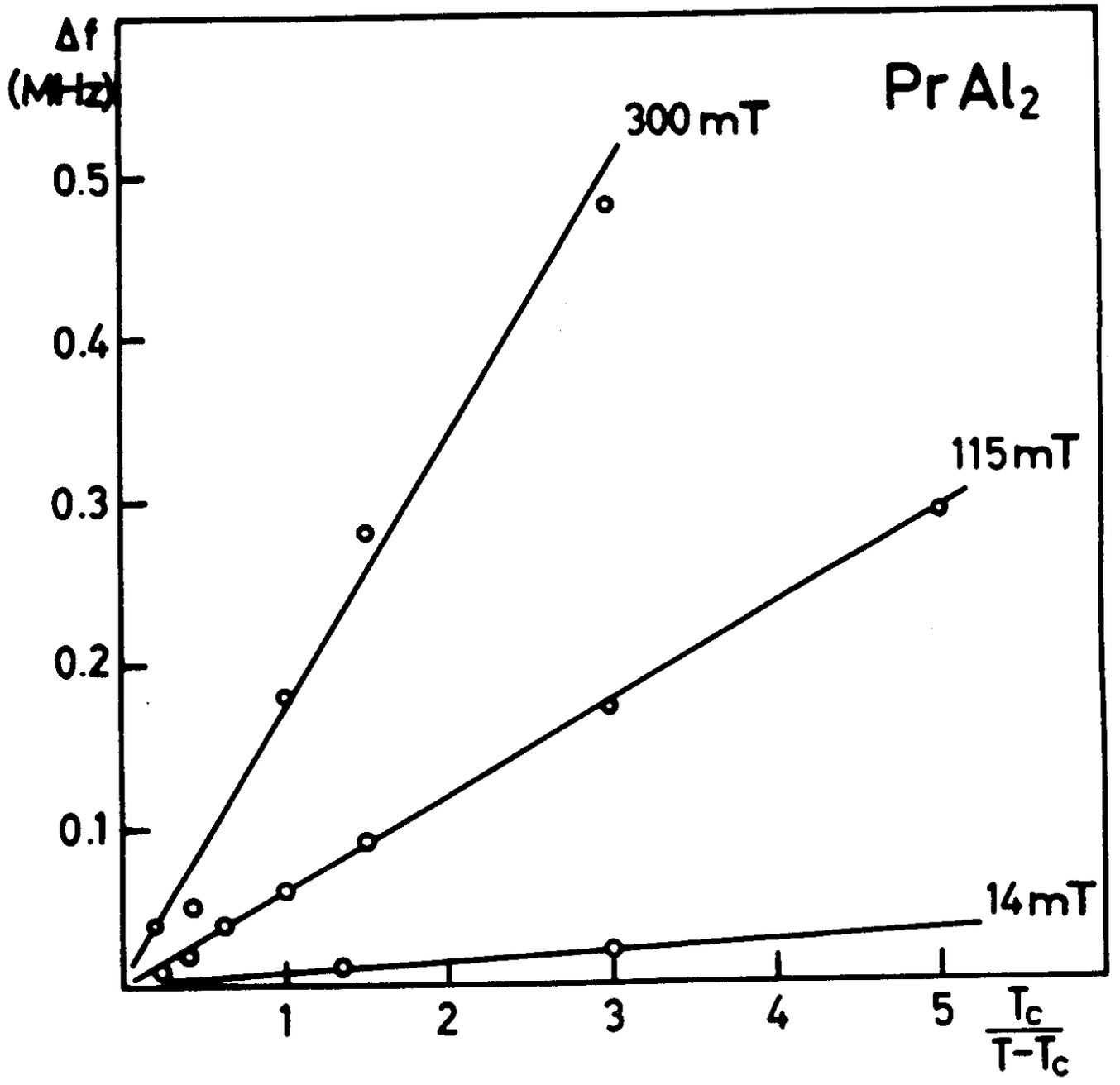

FIG.3

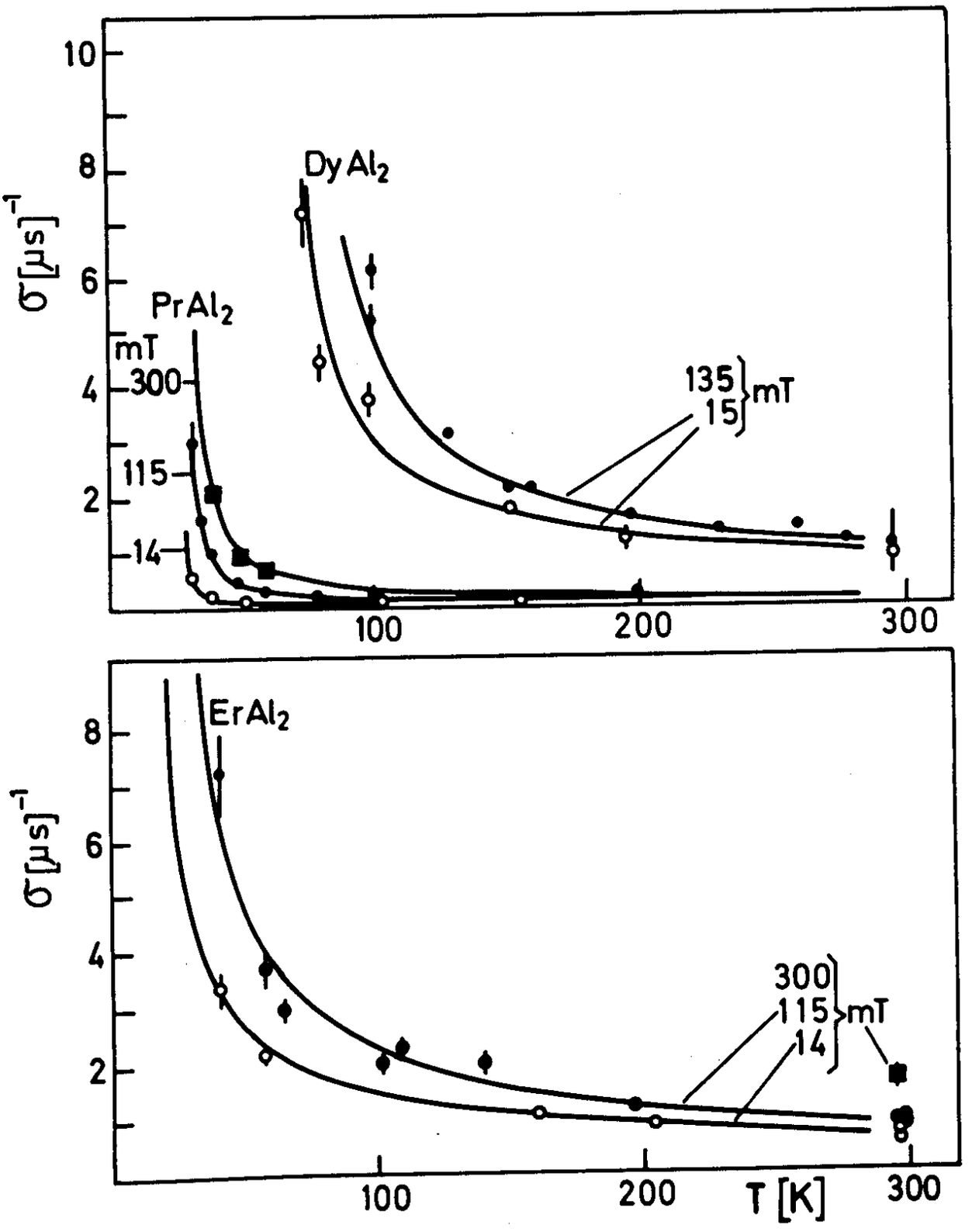
10
8
6
4
2
σ[μs]⁻¹
DyAl₂
PrAl₂
mT
300
115
14
135
15
mT
100
200
300
ErAl₂
300
115
14
mT
T [K]

FIG.4

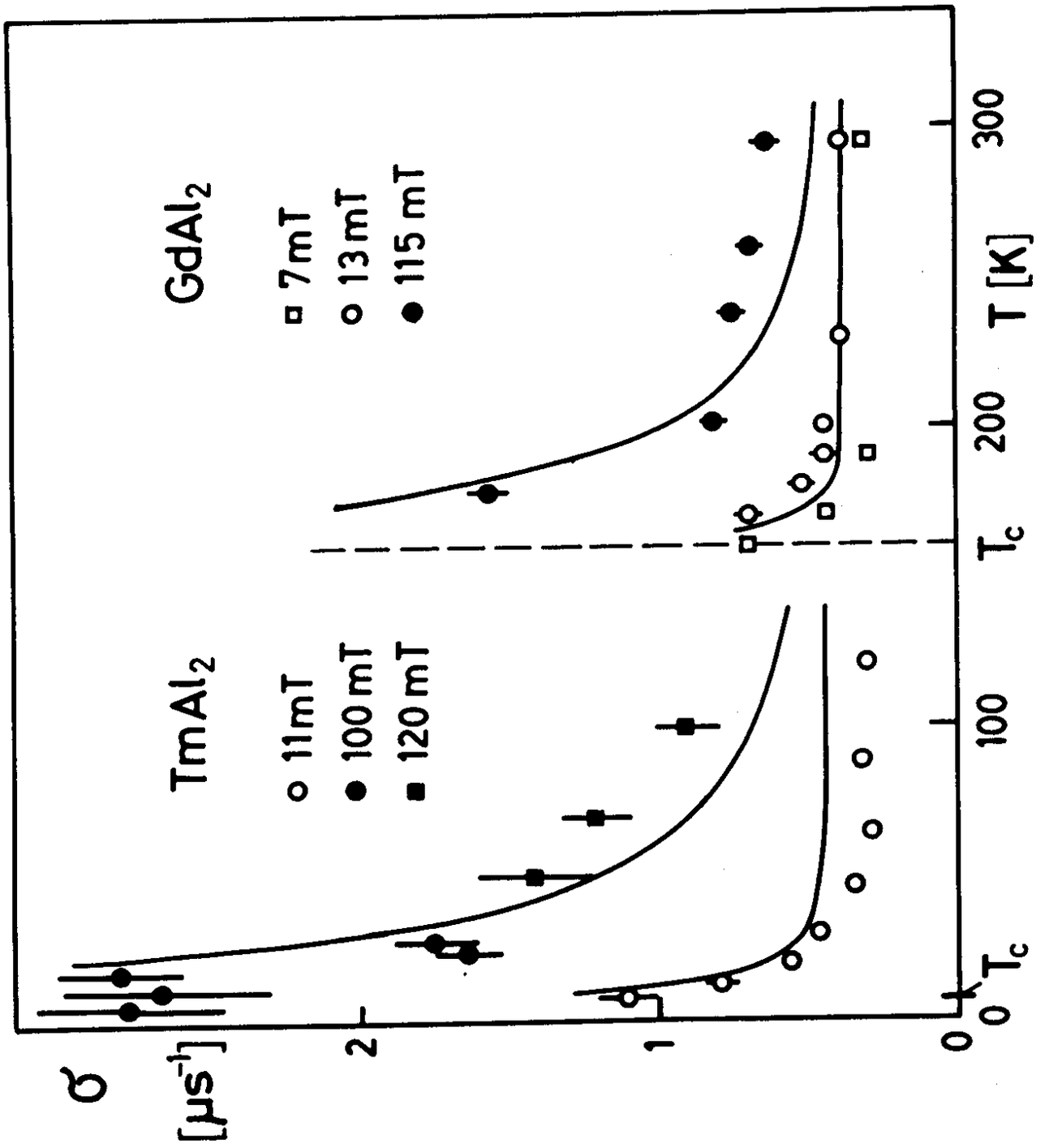
σ
[μs⁻¹]
2
1
0
0
Tc
100
TmAl2
11mT
100 mT
120 mT
GdAl2
7mT
13mT
115 mT
Tc
200
300
T [K]

FIG.5

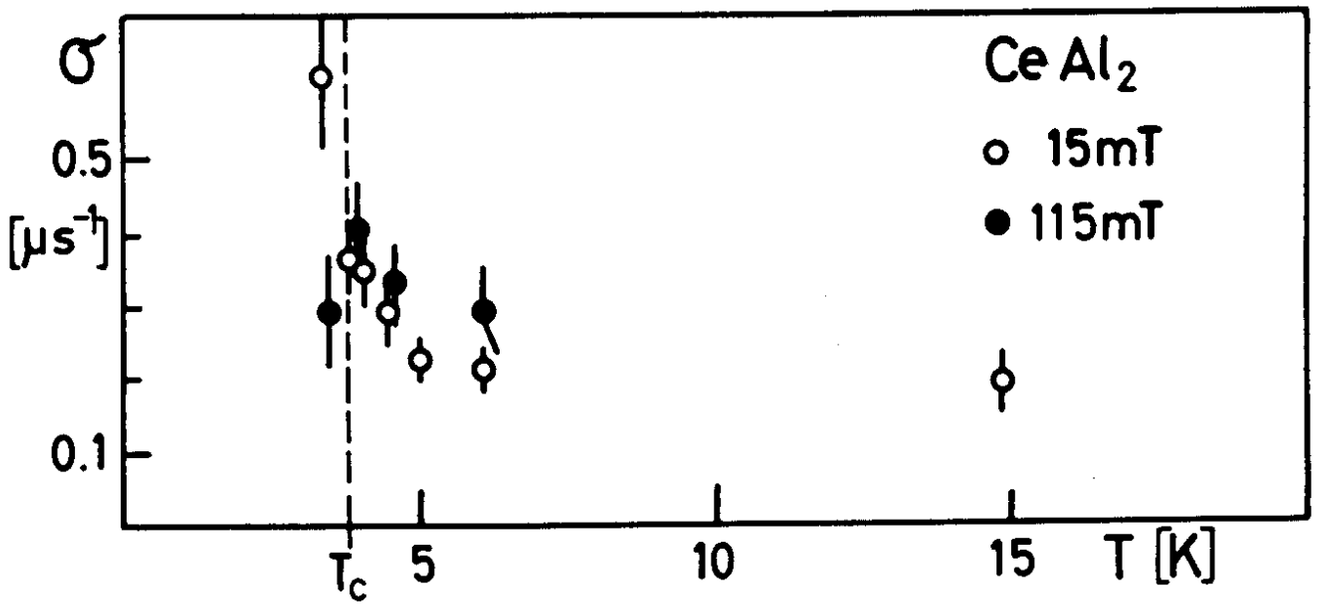
σ
0.5
[μs⁻¹]
0.1
Ce Al₂
o 15mT
● 115mT
T_c
5
10
15
T [K]

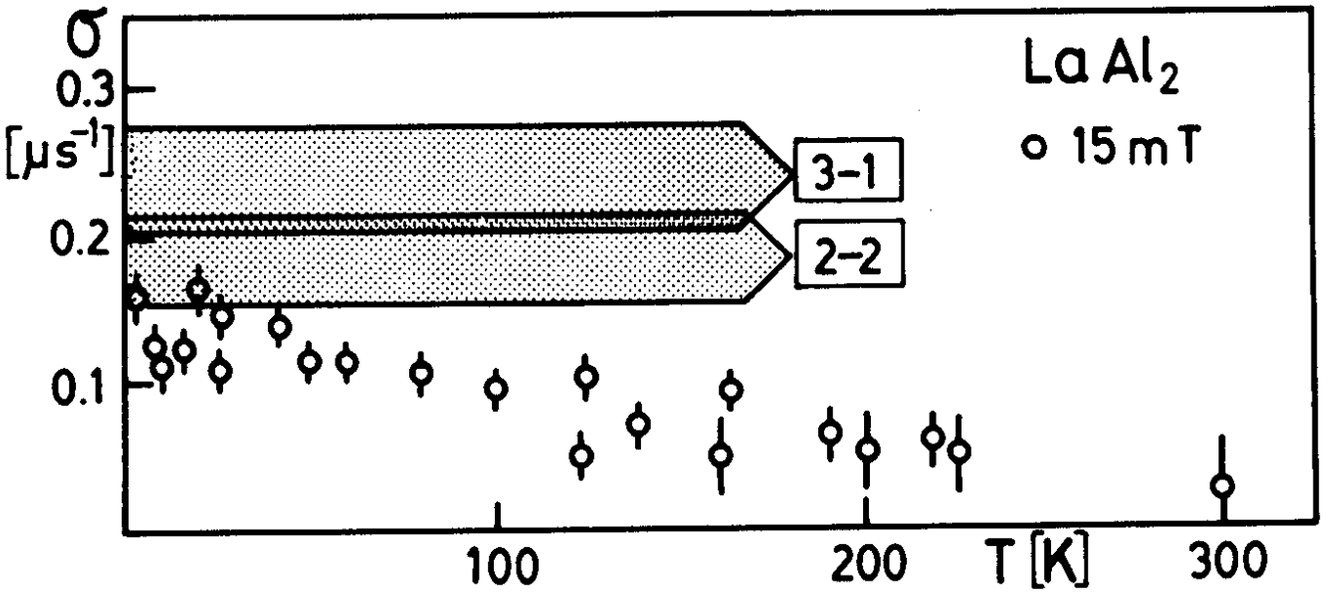
σ
0.3
[μs⁻¹]
0.2
0.1
La Al₂
o 15 mT
3-1
2-2
100
200
T [K]
300

FIG.6

FIG.7

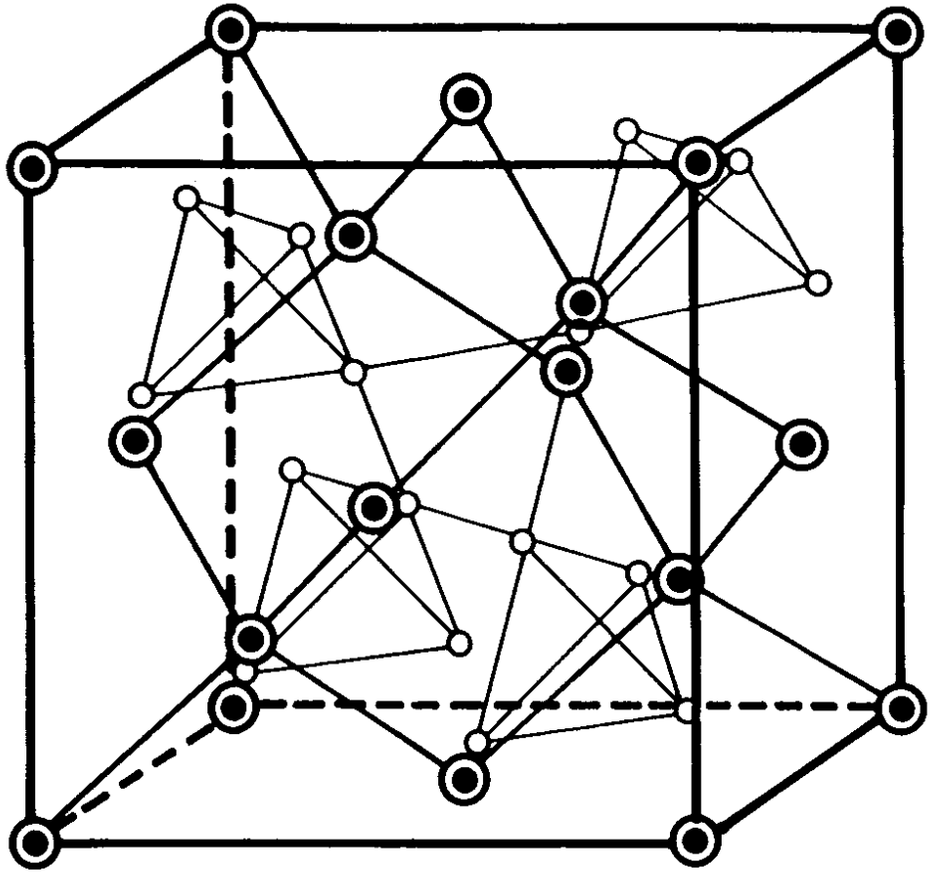

001 projection

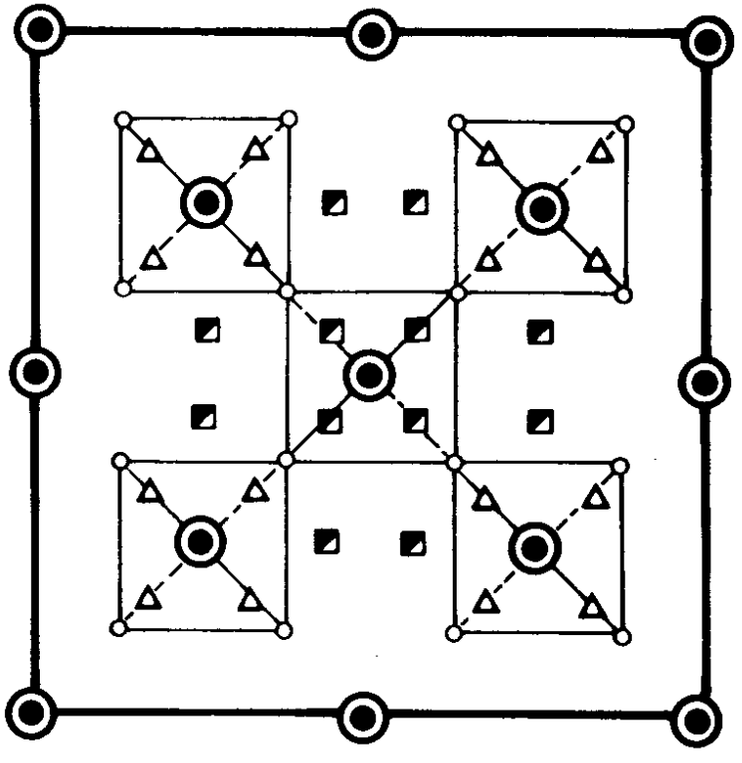

Rare Earth

Aluminum

2-2 muon position

3-1 muon position

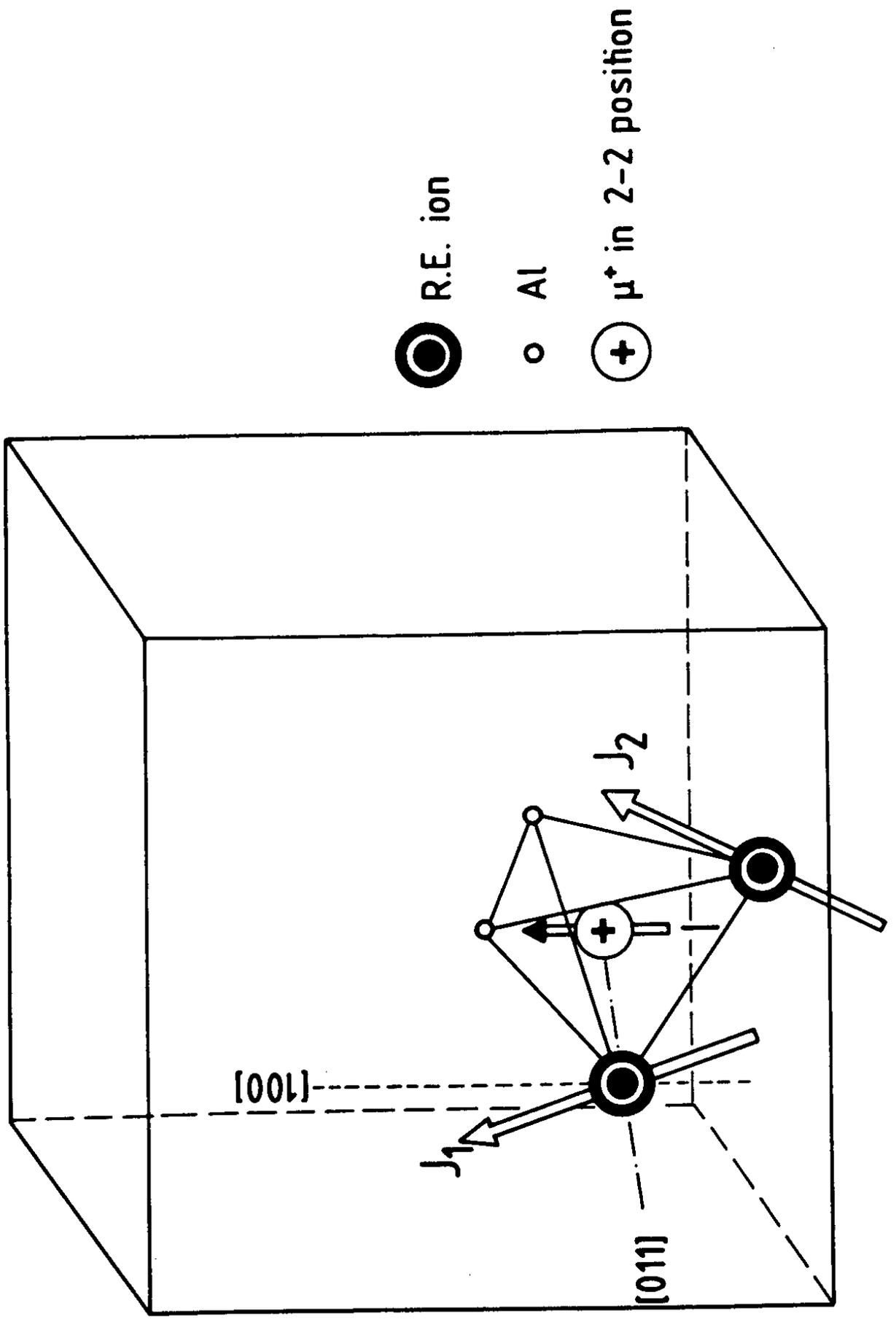

FIG.8

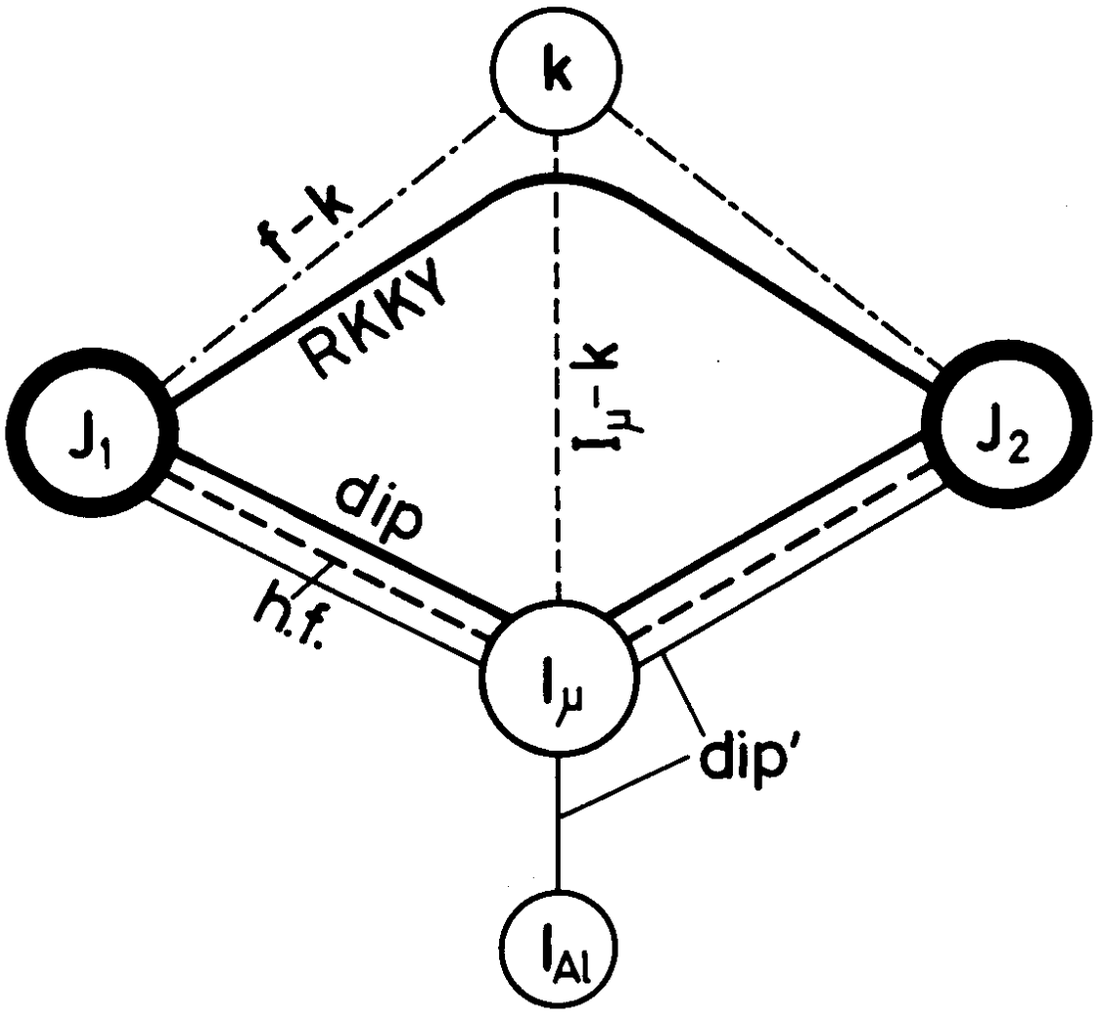

Magnetic interactions in $REAl_2$

I_μ = Muon spin

J_1, J_2 = RE (4f) angular momenta

k = Conduction electron spins

I_{Al} = Aluminum nuclear spin

dip = Electron dipolar interaction

dip' = Nuclear dipolar interaction

I_μ-k = Direct muon conduction el. interaction (weak)

FIG.9

0.1
-0.1
-0.2
-0.3
-0.4
-0.5
B_{cont} [T]
Pr
Nd
Sm
Eu
Gd
Tb
Dy
Ho
Er
Tm
C=−0.037 T
-0.1
-0.2
-0.3
-0.4
$B_{cont}=C(g_J-1)J$ [T]

FIG.10

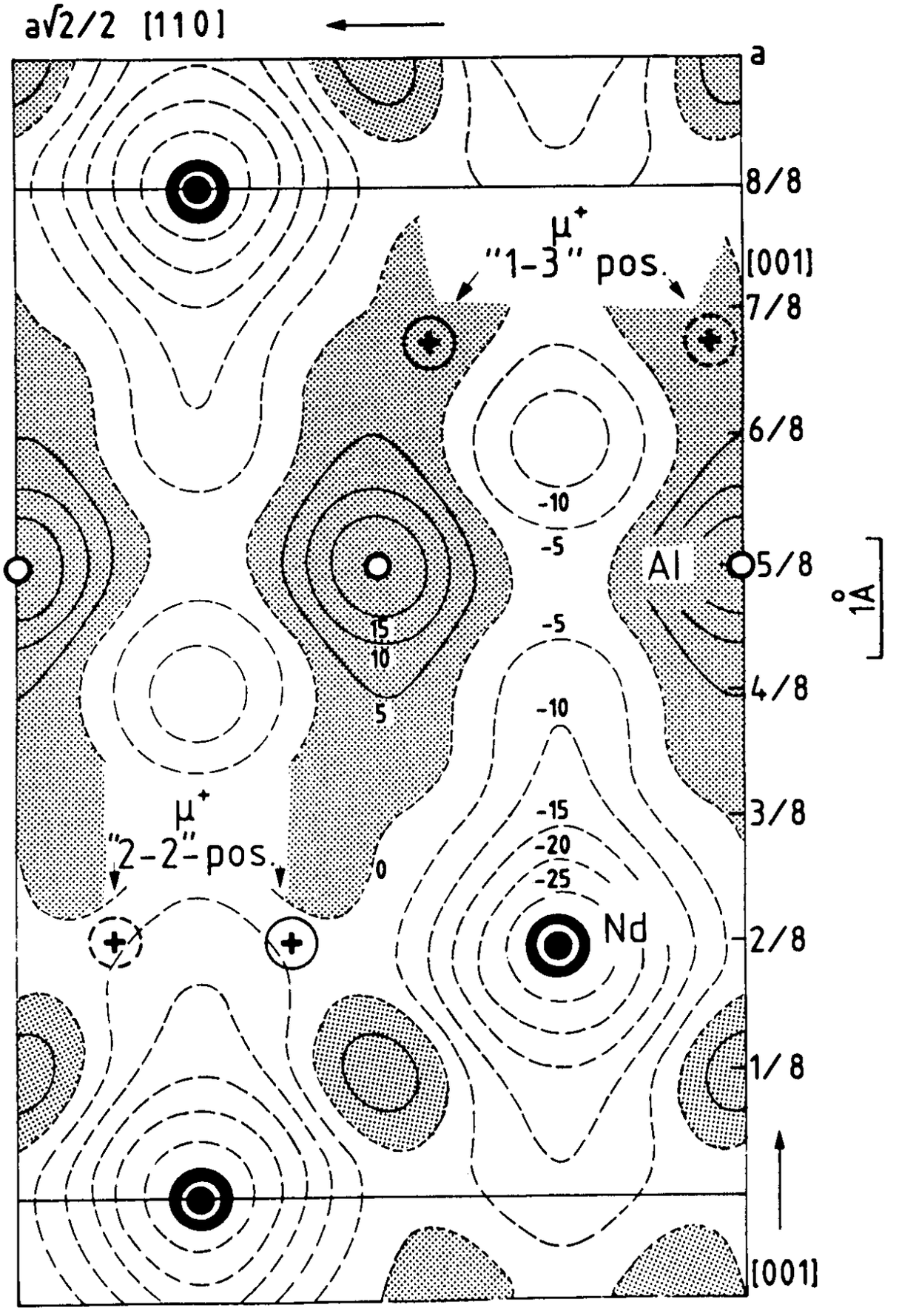
a√2/2 [110]
a
8/8
μ+
"1-3" pos.
[001]
7/8
6/8
-10
-5
Al
5/8
1Å
-5
15
10
5
4/8
-10
μ+
"2-2" pos.
-15
-20
-25
0
Nd
3/8
2/8
1/8
[001]

FIG.11

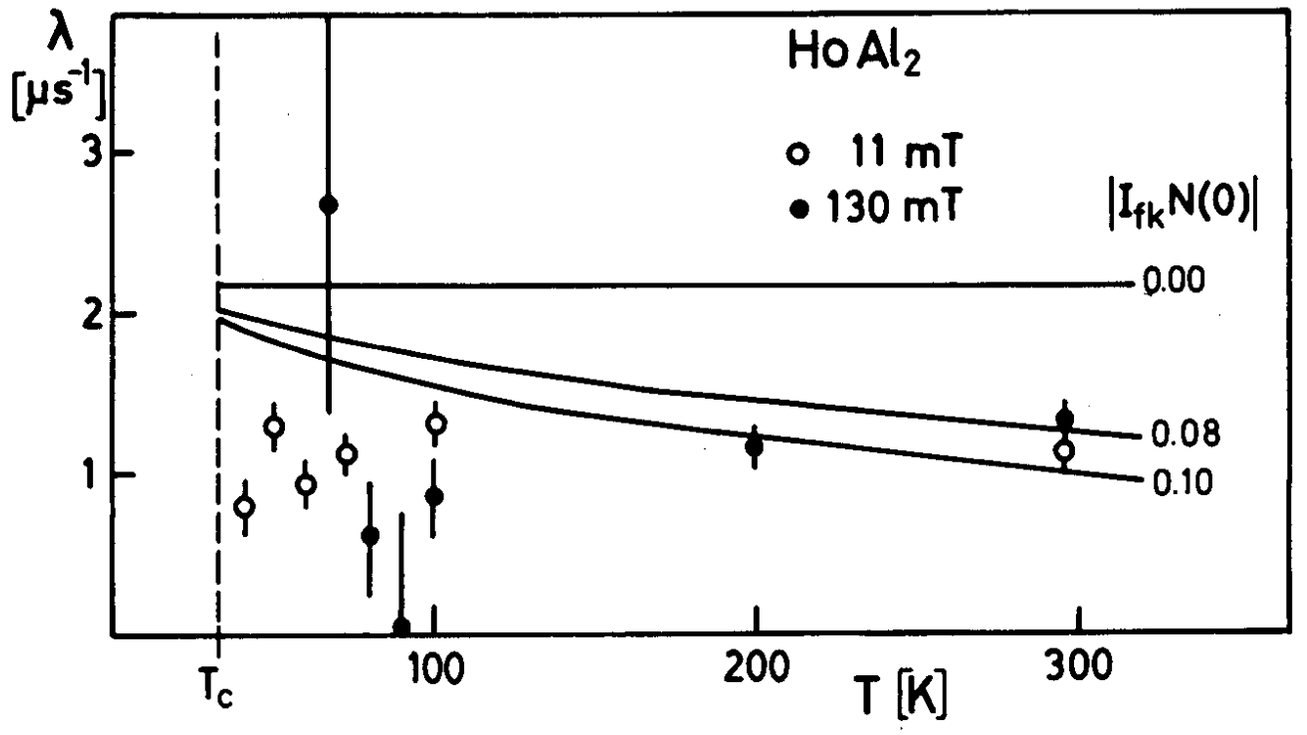
λ
[μs⁻¹]
HoAl2
11 mT
130 mT
|IfkN(0)|
0.00
0.08
0.10
3
2
1
Tc
100
200
300
T [K]

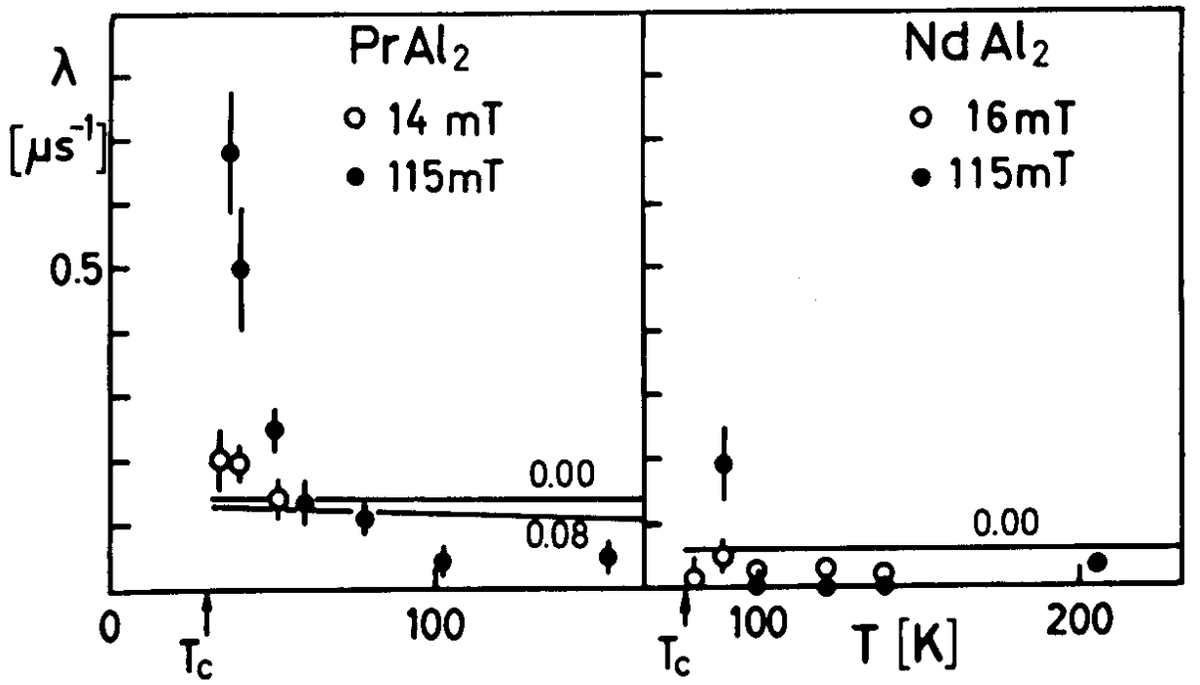
λ
[μs⁻¹]
PrAl2
14 mT
115mT
NdAl2
16mT
115mT
0.5
0.00
0.08
0.00
0
Tc
100
Tc
100
200
T [K]

FIG.12

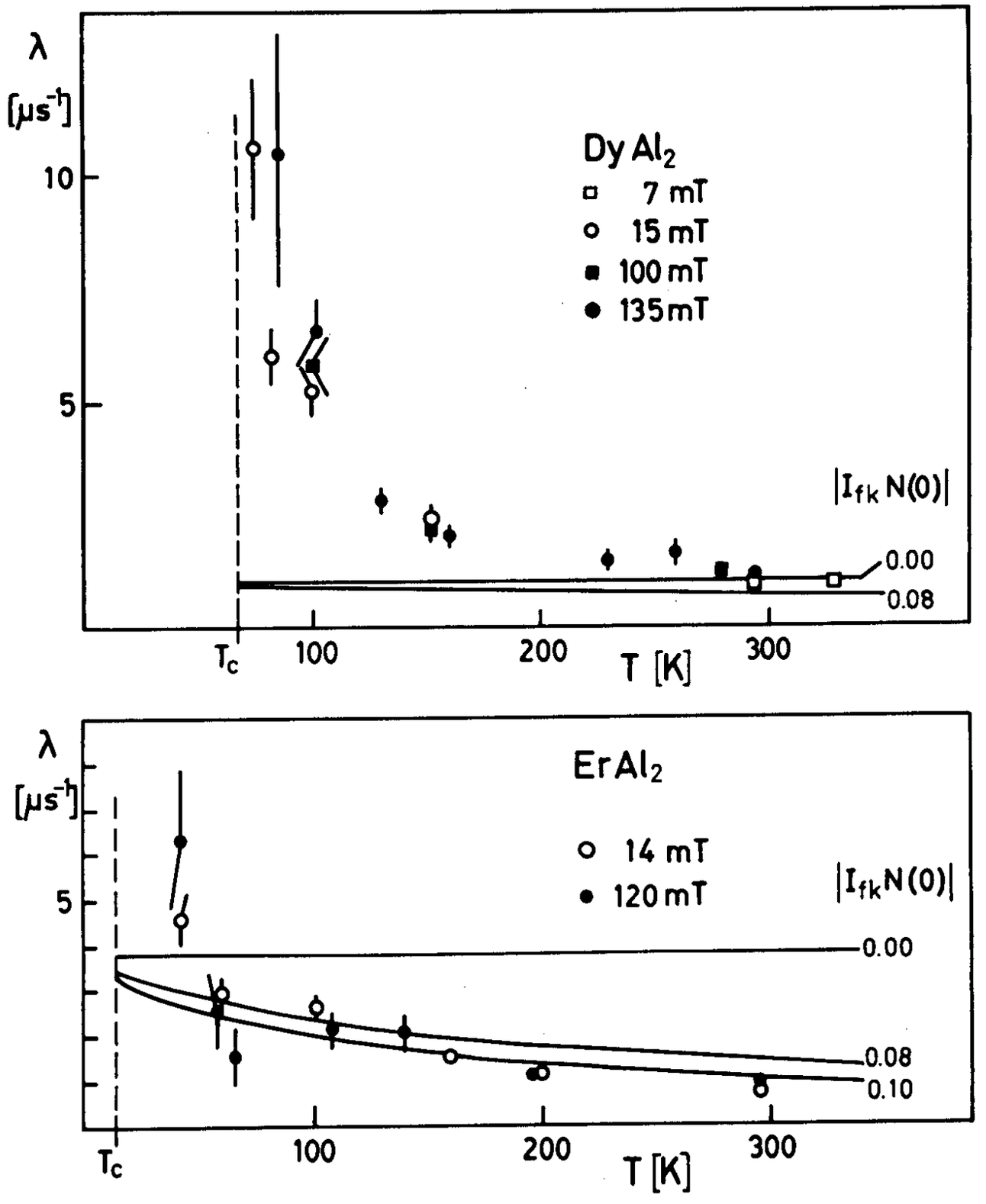
λ
[μs⁻¹]
10
5
Dy Al2
7 mT
15 mT
100 mT
135 mT
|Ifk N(0)|
0.00
0.08
Tc
100
200
300
T [K]
λ
[μs⁻¹]
5
Er Al2
14 mT
120 mT
|Ifk N(0)|
0.00
0.08
0.10
Tc
100
200
300
T [K]

FIG.13

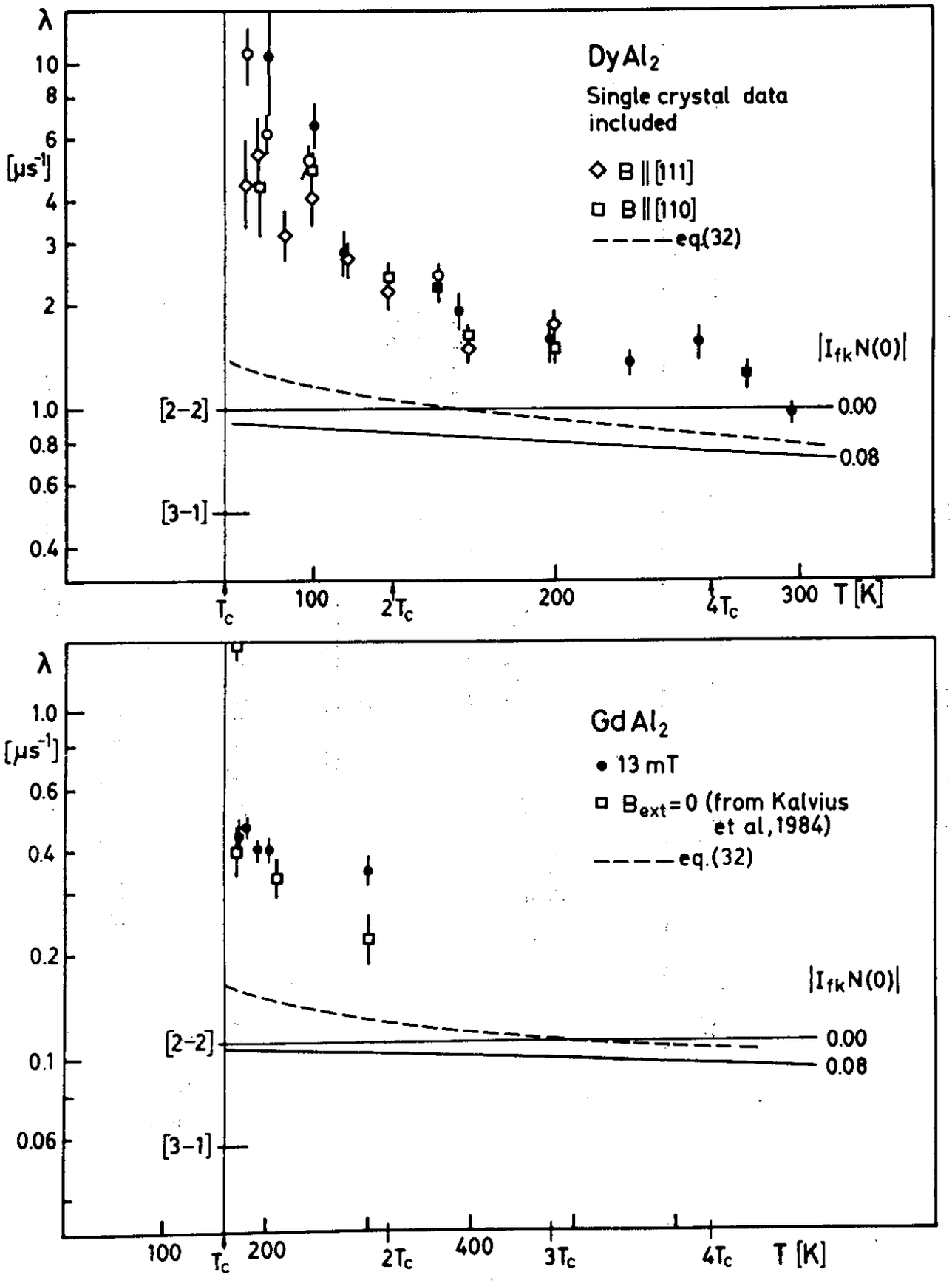
λ
10
8
6
[μs⁻¹]
4
3
2
1.0
0.8
0.6
0.4
DyAl2
Single crystal data included
◇ B ∥ [111]
□ B ∥ [110]
eq.(32)
|IfkN(0)|
[2-2]
0.00
0.08
[3-1]
Tc
100
2Tc
200
4Tc
300
T [K]
λ
1.0
[μs⁻¹]
0.6
0.4
0.2
0.1
0.06
GdAl2
• 13 mT
□ Bext=0 (from Kalvius et al,1984)
eq.(32)
|IfkN(0)|
[2-2]
0.00
0.08
[3-1]
100
Tc
200
2Tc
400
3Tc
4Tc
T [K]

FIG.14

FIG.15

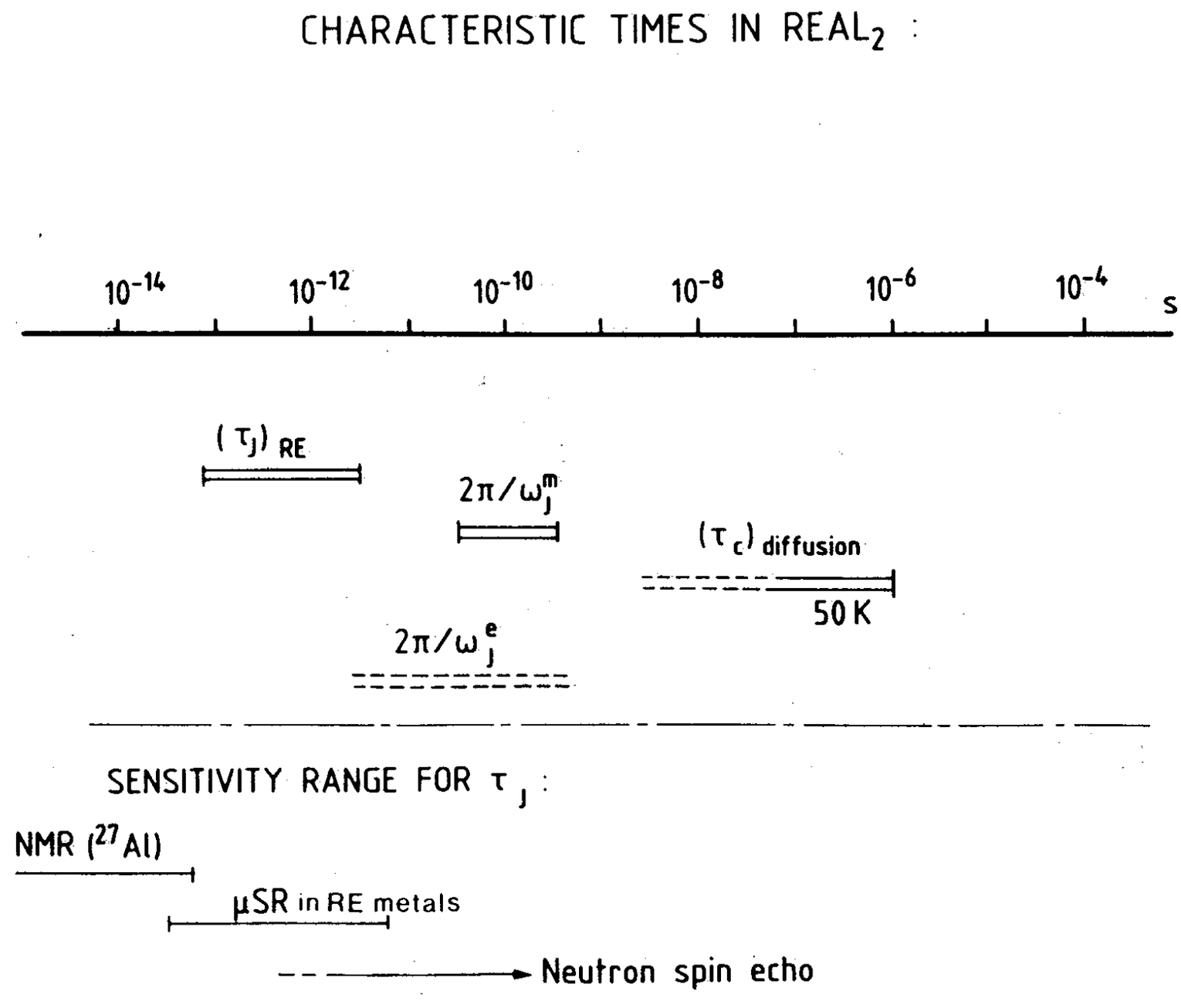
CHARACTERISTIC TIMES IN REAL2 :
10-14
10-12
10-10
10-8
10-6
10-4
s
(τJ) RE
2π/ωJm
(τc) diffusion
50 K
2π/ωJe
SENSITIVITY RANGE FOR τJ :
NMR (27Al)
μSR in RE metals
Neutron spin echo